PTEP

Prog. Theor. Exp. Phys. **2022** 013B13(30 pages)
DOI: 10.1093/ptep/ptab163

# Evaporation of black holes in flat space entangled with an auxiliary universe

Akihiro Miyata[1,*] and Tomonori Ugajin[2,3]

[1] *Institute of Physics, University of Tokyo, Komaba, Meguro-ku, Tokyo 153-8902, Japan*
[2] *Center for Gravitational Physics, Yukawa Institute for Theoretical Physics, Kyoto University, Kitashirakawa Oiwakecho, Sakyo-ku, Kyoto 606-8502, Japan*
[3] *The Hakubi Center for Advanced Research, Kyoto University, Yoshida Ushinomiyacho, Sakyo-ku, Kyoto 606-8501, Japan*
*E-mail: miyata@hep1.c.u-tokyo.ac.jp

Received October 12, 2021; Accepted December 10, 2021; Published December 14, 2021

We study a thermofield double type entangled state on two disjoint universes $A$ and $B$, where one of the universes is asymptotically flat containing a black hole. As we increase the entanglement temperature, this black hole receives back-reaction from the stress–energy tensor of the state. This results in lengthening of the wormhole region in the black hole interior, and decreasing of its horizon area, both of which are key features of an evaporating black hole. We then compute the entanglement entropy in universe $A$ through the island formula, and argue that it naturally follows the Page curve of an evaporating black hole in flat space. We also study the effects of local operations in the gravitating universe with the black hole. We find that they accelerate the evaporation of the black hole, thereby disrupting the entanglement between the two universes. Furthermore, we observe that, depending on whether the operation can be regarded as a local operation and classical communication or not, the behavior of the entanglement entropy changes. In particular, when the operation is made neither in the entanglement wedge of the radiation system nor that of the black hole, the transition between the island phase and the no-island phase can happen multiple times.

Subject Index B22

## 1. Introduction

Recently it has been claimed that in the presence of semi-classical gravity, the island formula gives the correct prescription to compute entanglement entropy [1–5]. This formula is inspired by the holographic entanglement entropy formula [6–8] and its quantum corrections [9,10] in the anti-de Sitter/conformal field theory (AdS/CFT) correspondence. When this formula is applied to a semi-classical black hole that is evaporating due to Hawking radiation, the entropy of the radiation naturally follows the Page curve [11,12]. This provides a resolution of the black hole information loss problem, and implies that semi-classical gravity is consistent with unitarity of quantum theory. The way in which this new rule provides the correct entropy involves a region called an "island" in the black hole. This island region naturally arises when we compute the entanglement entropy using a gravitational path integral through the replica trick [4,5]. In fact, the rule to evaluate a gravitational path in the semi-classical limit appears to include all saddles consistent with the given boundary conditions. It has been argued that there is an overlooked gravitational saddle in Hawking's calculation of the radiation entropy. This new saddle


Funded by SCOAP[3]

is called a replica wormhole, and this saddle gives the dominant contribution after the Page time. See Ref. [13] for a review of this topic.

One way to efficiently study black hole evaporation is by introducing another auxiliary universe, say universe $A$, which we assume to be non-gravitating, and consider an entangled state $|\Psi\rangle_{AB}$ on $A$ and the original gravitating universe $B$ with the black hole.[1] One can think of this new system as being generated out of the system in the single universe with an evaporating black hole, by gathering all Hawking quanta, and sending them to the auxiliary universe. Therefore the entanglement of $|\Psi\rangle_{AB}$ mimics that of the Hartle–Hawking state on the evaporating black hole. This setup has been used to study the entropy of Hawking radiation of 2D black holes in anti-de Sitter (AdS) space and de Sitter in JT gravity [28,29]. For studies with a similar approach, see Refs. [4,30]. Other applications of the island formula to de Sitter space can be found in Refs. [21,30–32]. Indeed, the entanglement entropy of this new system on $AB$ naturally follows a Page curve as a function of the entanglement temperature.

In this paper, we generalize this analysis to black holes in flat space. The evaporation of such 2D asymptotically flat black holes, as well as the time evolution of their radiation entropy, has been studied since the early 1990s [33–35]. Previous applications of the island formula to black holes in asymptotically flat space can be found, e.g., in Refs. [36–43]. Since the total state $|\Psi\rangle_{AB}$ induces the stress–energy tensor expectation value $\langle\Psi|T_{ab}|\Psi\rangle$ to the gravitating universe, the black hole in this universe receives a back-reaction from it. As in the cases of dS and AdS black holes in JT gravity, we show that this back-reaction is crucial to get the Page curve for the black hole in flat space. Two key effects of the back-reaction on the black hole are the following. First, it makes the wormhole in the interior region longer; second, it reduces the horizon area. This implies that, when we compute the entanglement entropy $S(\rho_A)$ of the non-gravitating universe using the island formula, it starts to decrease when the entanglement temperature is increased above some threshold value. This is in contrast to the case of AdS black holes, where the entropy is saturating to some constant value. The decrease in the entropy is plausible, because a black hole in flat space evaporates through Hawking radiation and loses its entropy.

We believe that our setup clarifies several ambiguities in the previous discussions on the island formula applied to asymptotically flat black holes. In the previous discussions, the radiation subsystem (the heat bath) is often naively taken to be the region $R$ located far away from the black hole, but it is still gravitating. However, such a choice for the radiation region $R$ is worrisome for several reasons. First, there is no consistent way to defined a "region" in the presence of gravity, in a diffeomorphism-invariant manner. In addition, the Hilbert space of quantum gravity never has a factorized into the Hilbert space on $R$ and its complement, due to the edge modes on the boundary of the region $R$. Second, when the heat bath is gravitating, the naive island formula is no longer valid, as has been shown in the recent papers [19,23,44,45]. This is because in the setup there is a novel wormhole connecting the gravitating bath and the black hole appearing in the path integral for the Rényi entropies. This is a concrete realization of the ER = EPR [46] conjecture, which predicts the existence of such a wormhole connecting the early radiation and the black hole interior.

These two concerns are avoided in a very clear manner in our setup of two disjoint universes. Namely, in our setup, since the radiation region is located on the non-gravitating universe $A$, which differs from the gravitating universe with the black hole, there is no ambiguity in defin-

[1] Another way to efficiently study the evaporation process is to holographically realize the system, by introducing branes on which gravitational degrees of freedom are living [1,4,14–27].

ing the radiation region in the first place. This in particular means that our definition of the entanglement entropy is unambiguous. Also, since the two universes in our setup are disjoint, we can safely turn off gravity in one of the universes; thus we do not need to worry about the existence of the wormhole connecting the bath and the black hole.

We then addressed the question of whether the entropy computed from the island formula is operationally meaningful from a quantum information theoretical point of view.To this end we study perturbations of the black hole by local operations in the gravitating universe. One way to model such a local operation is applying an operator well localized in the region of the interest, and this protocol is known as a local quench. The time evolution of the entanglement entropy in such quench processes has been extensively studied, e.g., in Refs. [47–57]. We find that such local operations "accelerate" the evaporation, especially when the operators are inserted in the interior of the black hole. The effects of such shock waves on the radiation entropy has been studied in Refs. [2,58–62] using the island formula.

We indeed find that our results obtained from the island formula are operationally meaningful. For instance, when the insertion is made either in the entanglement wedge of the radiation or in the similar wedge of the black hole, then the resulting entanglement entropies always decrease. This is consistent with the interpretation that such a local operator insertion is an LOCC (local operation and classical communication).

This paper is organized as follows. In Sect. 2 we explain our setup and the previous results for the island formula in this setup in detail. In Sect. 3, we introduce the black hole solution of interest and study how it is deformed due to the back-reaction of the stress–energy tensor expectation value of the total state. We then use the island formula to compute the entanglement entropy of the non-gravitating universe $A$. The result naturally follows a Page curve of an evaporating black hole. In Sect. 4, we study the Page curve in the presence of local operations in the gravitating universe. After classifying possible quantum extremal surfaces, we discuss the effects of the local operations on the entanglement entropy. We conclude this paper in Sect. 5. In Appendix A we review and discuss the time dependence of the entanglement entropy in a local quench in a 2D conformal field theory with a large central charge.

## 2. Setup

### 2.1 *Two disjoint asymptotically flat universes*

Let us first explain the setup that we consider in this paper. First of all, we prepare two disjoint universes, say $A$ and $B$, which are asymptotically flat (see Fig. 1). We then define two identical CFTs, one on each universe $A$ and $B$. For simplicity, in this paper, we only consider 2D spacetimes. Furthermore, we turn on semi-classical gravity in universe $B$. Thus the effective action of each universe reads

$$\log Z_A = \log Z_{\rm CFT}, \quad \log Z_B = -I_{\rm grav} + \log Z_{\rm CFT}. \tag{1}$$

As the gravitational part $I_{\rm grav}$ of the above effective action, we choose the CGHS action [33],

$$I_{\rm grav} = \frac{1}{4\pi}\int dx^2\sqrt{-g}\,(\Phi R - \Lambda)\,, \tag{2}$$

which is a theory of gravity in 2D asymptotically flat space. This action involves two fields, namely dilaton $\Phi$ and metric $g_{\mu\nu}$. Also, we introduced an auxiliary parameter $\Lambda$, for later purposes.[2]

[2]The reader should not confuse this parameter $\Lambda$ with a cosmological constant.

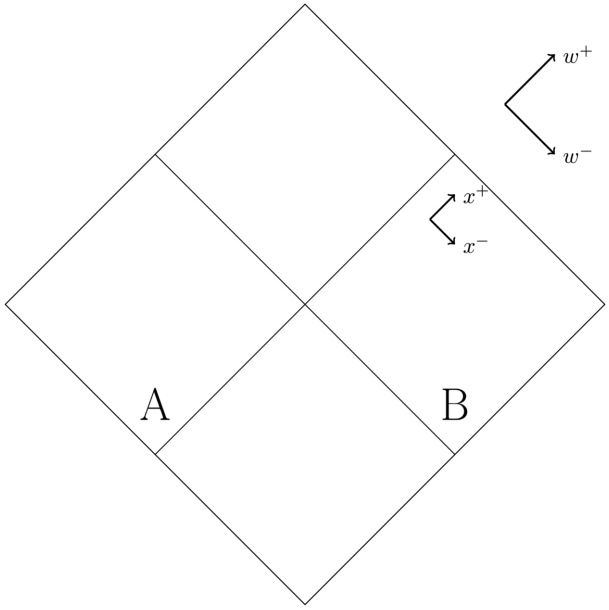


**Fig. 1.** We consider a system with two disjoint asymptotically Minkowski spaces, $A$ and $B$. In this figure, these universes are embedded in a larger Minkowski space.

The total Hilbert space of this system is naturally bipartite $H_A \otimes H_B$. Since these two universes $A$ and $B$ are disjoint, they cannot exchange classical information, but states on $A$ and $B$ can be entangled quantum mechanically. In this paper, we are interested in the structure of the entanglement of the states on the bipartite Hilbert space. To study this concretely, on the bipartite system we will consider the thermofield double (TFD) state:

$$|\Psi\rangle = \sum_{i=0}^{\infty} \sqrt{p_i}\, |i\rangle_A\, |\psi_i\rangle_B, \quad p_i = \frac{e^{-\beta E_i}}{Z(\beta)}, \tag{3}$$

where $Z(\beta)$ is a normalization factor that makes sure that the condition $\langle\Psi|\Psi\rangle = 1$, $|i\rangle_A$ is an energy eigenstate of the CFT on the non-gravitating universe $A$, and $|\psi_i\rangle_B$ is the same energy eigenstate on the gravitating universe $B$. Although they are identical states, since gravity is acting on universe $B$ and the properties of the state are affected by this, we instead write them differently. $\beta$ in Eq. (3) characterizes the amount of entanglement in this state. For this reason, $1/\beta$ is sometimes called the entanglement temperature.

### 2.2 *Islands in the setup*

In our previous papers [28,29], we studied the entanglement entropy $S(\rho_A)$ of the TFD state (3) on the non-gravitating universe $A$. This quantity is defined by the von Neumann entropy:

$$S(\rho_A) = -\mathrm{tr}\rho_A \log \rho_A, \quad \rho_A = \mathrm{tr}_B |\Psi\rangle\langle\Psi|. \tag{4}$$

This von Neumann entropy is computed by the replica trick; i.e., first compute the Rényi entropy $\mathrm{tr}\rho_A^n$, which has a path integral representation on the gravitating universe $B$, then at the end of the calculation send $n \to 1$. This gravitational path integral is evaluated in the semiclassical limit $G_N \to 0$ by including all saddles consistent with the given boundary conditions. In particular, by taking into account a wormhole that connects all replicas (replica wormhole), we obtained the following formula for the entanglement entropy:

$$S(\rho_A) = \min\{S_{\text{no-island}}, S_{\text{island}}\}. \tag{5}$$

$S_{\text{no-island}}$ in the above formula coincides with the CFT thermal entropy $S_{\text{no-island}} = S_\beta(B)$,

$$S_{\text{th}}(B) = -\sum_i p_i \log p_i, \tag{6}$$

with $p_i$ defined in Eq. (3). The other contribution $S_{\text{island}}$ in the above formula is given by taking the extremum of the generalized entropy,

$$S_{\text{island}} = \operatorname*{Ext}_{\bar{C}} \left[\Phi(\partial\bar{C}) + S_\beta[\bar{C}] - S_{\text{vac}}[\bar{C}]\right] \equiv \operatorname*{Ext}_{\bar{C}} S_{\text{gen}}[\bar{C}], \tag{7}$$

over all possible intervals $\bar{C}$ in the gravitating universe $B$. $\Phi(\partial\bar{C})$ is the "area term" of the generalized entropy, which is in the current case given by the sum of the dilaton values at the boundary of the interval $\bar{C}$. Also, $S_\beta[\bar{C}]$ is the entanglement entropy of thermal states on $\bar{C}$, and $S_{\text{vac}}[\bar{C}]$ is the entropy of the vacuum state. Since the TFD state is pure on the total system $AB$, the generalized entropy satisfies $S_{\text{gen}}[\bar{C}] = S_{\text{gen}}[AC]$. This implies that the interval $C$ in the gravitating universe $B$ can be identified with the island in our setup.

We are interested in the behavior of the entanglement entropy $S(\rho_A)$ as we tune the entanglement temperature $1/\beta$, especially when the gravitating universe $B$ contains a black hole. It has been argued that [28,29], in the low-temperature regime $\beta \gg 1$, since $S_{\text{no-island}} < S_{\text{island}}$ this entanglement entropy (5) coincides with the thermal entropy $S_{\text{th}}(B)$, which is an analogue of Hawking's result for the radiation entropy of evaporating black holes. Also, this implies that the entropy is linearly growing, as we increase the entanglement temperature $1/\beta$. At sufficiently high temperature $S_{\text{no-island}}$ is larger than $S_{\text{island}}$. According to the formula (5), in this regime the entanglement entropy is given by $S_{\text{island}}$, instead of the naive Hawking's entropy $S_{\text{no-island}}$. Furthermore, in this limit, $S_{\text{island}}$ almost coincides with the entropy of the black hole in the gravitating universe $B$. This is how the Page curve of an evaporating black hole is reproduced in the current setup.

### 2.3 *Embedding of two universes*

One way to study the setup is to embed the system in a larger Minkowski space $M$, as in Fig. 1. Each universe is a wedge in the larger space. The non-gravitating universe is the left wedge of $M$ and similarly the gravitating universe is the right wedge. To be more specific, let us define the light-cone coordinates $x^\pm = x \pm t$ on each universe. Also, let $(w^+, w^-)$ be the coordinates of the larger Minkowski space $M$. The embedding map is defined by

$$w^\pm = e^{\frac{2\pi}{\beta} x^\pm}. \tag{8}$$

The non-gravitating universe $A$ is mapped to the left wedge of $M$, $w^\pm < 0$, and the gravitating universe $B$ is mapped to the right wedge of $M$, $w^\pm > 0$. Also, the thermofield double state on $AB$ is mapped to the global Minkowski vacuum of $M$.

## 3. An asymptotically flat black hole and its radiation entropy

The purpose of this paper is to study a similar entropy in asymptotically flat spacetime using the island formula (5). To do so, we need to specify the dilaton profile $\Phi$ that appears in the generalized entropy (7). Since the thermofield double state induces the thermal stress–energy tensor expectation value $\langle\Psi|T_{\pm\pm}|\Psi\rangle$ on the gravitating universe $B$, this dilaton receives a back-reaction from it.

In the CGHS model with the action (2), the metric is always fixed to the flat one, as the variation of the action with respect to $\Phi$ sets $R = 0$. We will find it convenient to use the compact

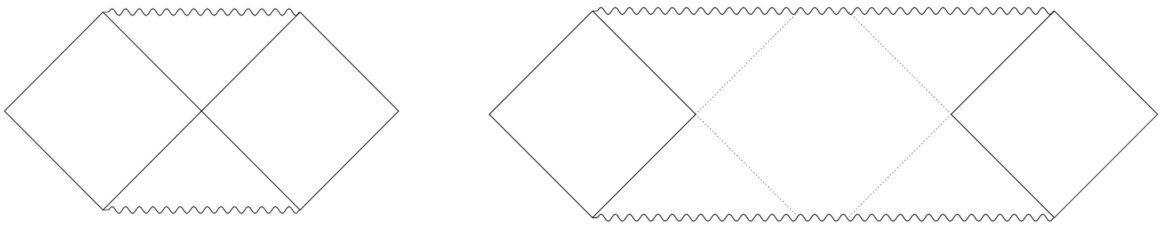

**Fig. 2.** Left: A Penrose diagram of the black hole without the back-reaction. Right: A Penrose diagram of the black hole with the back-reaction of the source (14). It develops a long wormhole region in its interior.

coordinates $(x^+, x^-)$, in which the flat metric is given by

$$ds^2 = -\frac{dx^+ dx^-}{\cos^2 x^+ \cos^2 x^-}, \quad -\frac{\pi}{2} \leq x^\pm \leq \frac{\pi}{2}. \tag{9}$$

These coordinates are related to the standard coordinates $(X^+, X^-)$ with the metric $ds^2 = -dX^+ dX^-$ by $X^\pm = \tan x^\pm$. In the coordinate system, $x^+ = \pm\frac{\pi}{2}$ and $x^- = \pm\frac{\pi}{2}$ correspond to asymptotic infinities of the spacetime.

The equations of motion for the dilaton are given by

$$\nabla_a \nabla_b \Phi - g_{ab} \nabla^2 \Phi = \frac{\Lambda}{2} g_{ab} - 2\pi \ \langle \Psi | T_{ab} | \Psi \rangle. \tag{10}$$

In general, in the light-cone gauge where the metric takes the form

$$ds^2 = -e^{2\omega} dx^+ dx^-, \tag{11}$$

these equations of motion are reduced to

$$-e^{2\omega} \partial_\pm \left[ e^{-2\omega} \partial_\pm \right] \Phi = 2\pi \ \langle \Psi | \ T_{\pm\pm} | \Psi \rangle, \quad \partial_+ \partial_- \Phi = 2\pi \ \langle \Psi | T_{+-} | \Psi \rangle + \frac{\Lambda}{4} e^{2\omega}. \tag{12}$$

### 3.1 *The sourceless solution*

Let us first discuss the dilaton profile when the stress–energy tensor is vanishing $\langle \Psi | T_{ab} | \Psi \rangle = 0$. In our setup, this happens when the entanglement temperature is low, $\beta \to \infty$. It reads

$$\Phi_0 = \phi_0 + \frac{\Lambda}{4} \tan x^+ \tan x^-, \tag{13}$$

where $\Lambda$ is the parameter in the CGHS action (2). As we will see, this dilaton profile corresponds to an asymptotically flat eternal black hole, whose Penrose diagram is identical to the standard 4D Schwarzschild eternal black hole (refer to the left panel of Fig. 2).

### 3.2 *The solution with the source*

As we increase the entanglement temperature, it is no longer possible to neglect the back-reaction of the stress–energy tensor to the dilaton profile. The stress–energy tensor expectation value of the thermofield double state (3) is

$$\langle \Psi | T_{\pm\pm} | \Psi \rangle = \frac{c}{24\pi} \left( \frac{2\pi}{\beta} \right)^2. \tag{14}$$

By solving Eqs. (12) for $\Phi$, we get

$$\Phi_\beta = \phi_0 + \frac{\Lambda}{4} \tan x^+ \tan x^- - X_\beta \left( x^+ \tan x^+ + x^- \tan x^- \right), \quad X_\beta \equiv \frac{c}{24} \left( \frac{2\pi}{\beta} \right)^2. \tag{15}$$

This solution corresponds to an eternal black hole with a long interior region (the right panel of Fig. 2).

### 3.3 *Penrose diagrams*

Having presented the dilaton profile of interest (15), let us now discuss the causal structure of the spacetime described by the profile. Since it turns out that it corresponds to an eternal black hole, we are interested in the location of the singularity and the event horizon. A useful fact is that the dilaton is vanishing $\Phi = 0$ at the black hole singularity. Also, the bifurcation surface of the black hole is a critical point $\partial_\pm \Phi = 0$. The entropy of the black hole is given by the dilaton value at the critical point.

3.3.1 *The sourceless solution.* As a warm-up, let us describe the causal structure of the dilaton profile (13) without the source. In this case, the location of the singularity satisfies

$$\Phi_0 = 0 \leftrightarrow \tan x^+ \tan x^- = -\frac{4\phi_0}{\Lambda}. \tag{16}$$

In the standard coordinates $(X^+, X^-)$, this singularity is just a hyperbola $X^+X^- = -4\phi_0/\Lambda$, which is expected. This singularity intersects with the right future null infinity $x^+ = \frac{\pi}{2}$ at $x^- = 0$. Similarly, it intersects with the left future infinity $x^- = -\frac{\pi}{2}$ at $x^+ = 0$. This fixes the location of the event horizon to $x^+ = 0$ and $x^- = 0$. Indeed, this black hole has only one bifurcation surface, i.e., at $x^\pm = 0$. The value of the dilaton at the bifurcation surface is $\Phi(0) = \phi_0$, which is equal to the entropy of the black hole, and is independent of $\Lambda$.

3.3.2 *The solution with the source.* The structure of the spacetime is eventually deformed by turning on the stress–energy tensor (14), due to the back-reaction, which is described by the dilaton profile $\Phi_\beta$ (15). We can read off the location of the singularity in the deformed spacetime from $\Phi_\beta$. Near the right future null infinity $x^+ = \frac{\pi}{2}$, the dilaton profile is approximated as

$$\Phi_\beta = \frac{\Lambda}{4} \tan x^+ \left( \tan x^- - \frac{2\pi X_\beta}{\Lambda} \right), \quad x^+ \to \frac{\pi}{2}. \tag{17}$$

Therefore, the singularity intersects with the future infinity at $x^- = x_c^-$ with

$$\tan x_c^- = \frac{2\pi X_\beta}{\Lambda}. \tag{18}$$

As we increase the entanglement temperature $\beta \to 0$, $X_\beta$ on the right-hand side gets large and the intersection approaches spatial infinity, $x_c^- \to \frac{\pi}{2}$ with $x^+ = \frac{\pi}{2}$. Similarly, the singularity intersects with the left future null infinity $x^- = -\frac{\pi}{2}$ at $x^+ = x_c^+$ with

$$\tan x_c^+ = -\frac{2\pi X_\beta}{\Lambda}, \tag{19}$$

again in the high-temperature limit; it satisfies $x_c^+ \to -\frac{\pi}{2}$, so this intersection approaches the opposite spatial infinity. Since the dilaton profile (15) is invariant under time reflection $x^+ \leftrightarrow x^-$, the singularity intersects with the past null infinity in a similar fashion. Namely, it intersects with the right past null infinity $x^- = \frac{\pi}{2}$ at $x^+ = -x_c^+$ with Eq. (19) and the left past null infinity $x^+ = -\frac{\pi}{2}$ at $x^- = -x_c^-$ with Eq. (18). In summary, as one increases the entanglement temperature, the singularity of the black hole comes close to the reflection symmetric slice $x^+ = x^-$.

This also fixes the location of the event horizon of the black hole. The right future horizon of the black hole is at $x^- = x_c^-$ with Eq. (18). Similarly, the left future horizon is at $x^+ = -x_c^+$. Since these two future horizons do not intersect on the reflection symmetric slice $x^+ = x^-$, this black hole contains a region in its interior that is causally inaccessible from asymptotic infinities (the right panel of Fig. 2). Such a region is called a causal shadow region. The fact that the

black hole singularity approaches the reflection symmetric slice as we increase the entanglement temperature means that the causal shadow region gets larger and larger in this limit.

One can also confirm this by finding locations of the bifurcation surfaces $(x_H^+, x_H^-)$ that satisfy $\partial_\pm \Phi_\beta = 0$. Because of the symmetry $x^+ \leftrightarrow x^-$ of the dilaton profile (15), these bifurcation surfaces satisfy $x_H^+ = x_H^- \equiv y$, and

$$\frac{\Lambda}{4}\tan y - X_\beta\,(\cos y \sin y + y) = 0. \tag{20}$$

We are interested in the $\beta \to 0$ limit, where the two solutions $y = y_\pm$ of Eq. (20) satisfy

$$\tan y_\pm = \frac{4X_\beta y_\pm}{\Lambda}. \tag{21}$$

Both of these bifurcation surfaces get close to the spatial infinity, $y_\pm \to \pm\frac{\pi}{2}$. The dilaton value at these bifurcation surfaces in the same limit is given by

$$\Phi_\beta(x_H^\pm) = \phi_0 - \frac{(\pi X_\beta)^2}{\Lambda}. \tag{22}$$

Notice that the dilaton value $\Phi_\beta(x_H^\pm)$ at the horizon decreases as we increase $1/\beta$. This means that, as we increase the entanglement between the two universes $\beta \to 0$, the back-reaction of the CFT stress–energy tensor makes the horizon area of the black hole smaller. This is closely related to the fact that, quantum mechanically, a black hole in flat space evaporates by the emission of Hawking quanta. Indeed, our setup can be regarded as an idealization of the black hole plus a radiation system. The radiation degrees of freedom are modeled by the CFT degrees of freedom in our setup, and the entanglement of the CFT thermofield double state between $A$ and $B$ is the avatar of the entanglement in the Hartle–Hawking state. Therefore the increase of the entanglement of the TFD state (which we do by hand) captures the late time physics of the actual black hole evaporation process, and as a result the black hole in our setup loses its entropy.

We cannot have a semi-classical description of the black hole at the very final stage of evaporation. This is because, as we increase the entanglement temperature, both future and past singularities come close to the reflection symmetric slice, and eventually touch the slice. This critical temperature can also be read off from the dilaton values at the bifurcation surfaces (22), where it becomes zero.

### 3.4 *Quantum extremal surfaces*

Now, let us compute the entanglement entropy $S(\rho_A)$ of universe $A$ through the island formula (5) with Eq. (7). For this purpose we need to extremize the generalized entropy for all possible intervals $\bar{C}$ whose end points are identified with quantum extremal surfaces. In the calculation, it is reasonable to assume that $\bar{C}$ is on the reflection symmetric slice $x^+ = x^-$, and is given by the union of two intervals $\bar{C} = \bar{C}_1 \cup \bar{C}_2$, $\bar{C}_1 : -\frac{\pi}{2} < x^+ \le -\frac{\pi x}{2}$, $\bar{C}_2 : \frac{\pi x}{2} \le x^+ < \frac{\pi}{2}$ with $0 < x < 1$. The generalized entropy reduces to a function of a single variable $x$,

$$S_{\rm gen}(x) = 2\Phi_\beta(x) + \frac{2c}{3}\log\left[\frac{\beta}{\pi\varepsilon_{\rm UV}}\sinh\frac{\pi^2}{2\beta}(1-x)\right] - \frac{2c}{3}\log\left[\frac{1}{\varepsilon_{\rm UV}}\sin\frac{\pi}{2}(1-x)\right], \tag{23}$$

where $\varepsilon_{\rm UV}$ is the UV cutoff. We show a plot of the above function in Fig. 3.

In the $\beta \to 0$ limit, the quantum extremal surfaces (QESs) almost coincide with the classical bifurcation surfaces of the black hole. This is because the QESs approach the spatial infinity and therefore the CFT entropy part in $S_{\rm gen}(x)$ is vanishing in this limit. As a result, the island is identified with the causal shadow region in the black hole interior (Fig. 4).

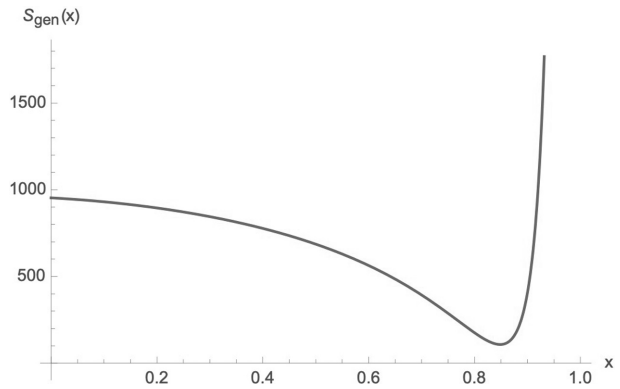


**Fig. 3.** Plot of the generalized entropy $S_{\text{gen}}(x)$ as a function of the size of the island in the interior. Here we set the parameters to be $\phi_0 = 1700$, $\Lambda = 500$, $c = 50$ and $\beta = 1$.

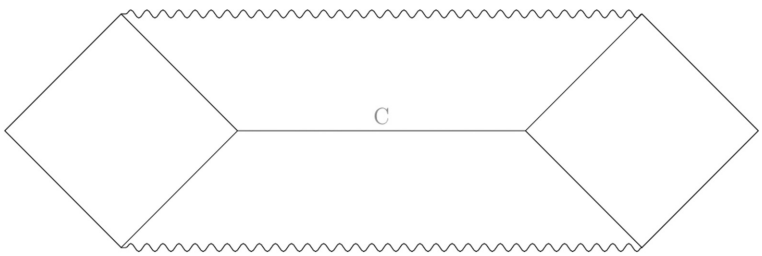


**Fig. 4.** The location of the island $C$ in the black hole with the back-reaction, denoted by the blue line.

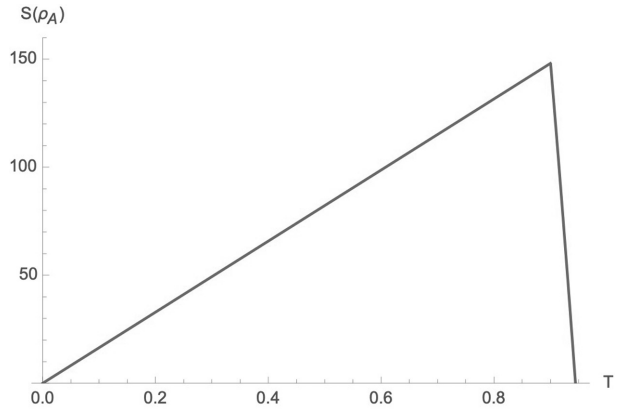


**Fig. 5.** The resulting Page curve as a function of the entanglement temperature $T = 1/\beta$. Here we set the parameters to be $\phi_0 = 1700$, $\Lambda = 500$ and $c = 50$.

By combining these results, we get the following approximate expression for the entanglement entropy $S(\rho_A)$:

$$S(\rho_A) = \begin{cases} S_{\text{no-island}} = \frac{\pi^2 c}{3\beta} & \beta > \beta_c \\ S_{\text{island}} = 2\left[\phi_0 - \frac{(\pi X_\beta)^2}{\Lambda}\right] & \beta < \beta_c, \end{cases} \tag{24}$$

where $\beta_c$ is the critical inverse temperature satisfying $S_{\text{no-island}} = S_{\text{island}}$. We plot the Page curve by using the above expression in Fig. 5.

## 4. Black hole interior in the presence of a shock wave

We have seen that, by making the entanglement between the two universes stronger, the size of the black hole interior in the gravitating universe $B$ gets larger. So in some sense this interior region is created by the entanglement between the degrees of freedom in the gravitating universe $B$ and those in the other (non-gravitating) universe. To sharpen the intuition, in this section, we would like to ask how the local operations in the gravitating universe $B$ change the entanglement.

We imagine that an experimental physicist in a laboratory has this system $AB$ of two disjoint universes (or the larger Minkowski space containing $AB$ as in Fig. 1), and can perform any local operation on the gravitating universe $B$ even in the black hole interior. Such local operations can be modeled by a shock wave in the null directions along which the CFT stress–energy tensor has a delta functional peak. Such a peak of the stress–energy tensor can back-react to the dilaton profile through the equations of motion (12).

We start from the state $|\Psi\rangle$ on $AB$, prepared by inserting a local operator $\mathcal{O}_B$ in the gravitating universe $B$ to the thermofield double state:

$$|\Psi\rangle = (1_A \otimes \mathcal{O}_B)|\mathrm{TFD}\rangle = \frac{1}{\sqrt{Z(\beta)}} \sum_{i=0}^{\infty} e^{-\frac{\beta}{2}E_i} \, |i\rangle_A \, \otimes \mathcal{O}_B \, |\psi_i\rangle_B. \tag{25}$$

We are interested in its entanglement entropy $S(\rho_A)$ of the above state, which is computed by the island formula (5). Since $S_{\text{no-island}}$ does not change by the insertion of $\mathcal{O}_B$, we focus on $S_{\text{island}}$ given by the generalized entropy,

$$S_{\text{gen}} = \mathrm{Ext}_{\bar{C}} \left[ \Phi(\partial \bar{C}) + S_{\beta,E}[\bar{C}] - S_{\text{vac}}[\bar{C}] \right], \tag{26}$$

where $S_{\beta,E}[\bar{C}]$ denotes the CFT entanglement entropy in the presence of the shock wave created by $\mathcal{O}_B$.

Let $(x_0^+, x_0^-)$ be the location of the insertion of the operator $\mathcal{O}$. Then the reduced density matrix of universe $B$ is

$$\rho = \mathrm{tr}_A |\Psi\rangle\langle\Psi| = \frac{1}{Z_{\mathcal{O}}} \, e^{-\varepsilon H} \mathcal{O}\left(x_0^+, x_0^-\right) \rho_\beta \, \mathcal{O}^\dagger\left(x_0^+, x_0^-\right) \, e^{-\varepsilon H}. \tag{27}$$

Here we introduced a UV regulator $\varepsilon$, to make the density matrix normalizable, and the normalization factor

$$Z_{\mathcal{O}} = \langle \mathcal{O}(2i\varepsilon)\mathcal{O}(0)\rangle_\beta, \tag{28}$$

which ensures $\mathrm{tr}\,\rho = 1$. We also denote $\langle \cdots \rangle_\beta \equiv \mathrm{tr}[\rho_\beta \cdots]$.

This local operator $\mathcal{O}$ affects the stress–energy tensor expectation value and therefore the dilaton profile. The stress–energy tensor expectation value can be computed by the three-point functions $\mathrm{tr}[\rho_\beta T_{\pm\pm}\mathcal{O}\mathcal{O}]$, and it reads

$$\begin{aligned} \langle \Psi | T_{++}(x^+) | \Psi \rangle &= \frac{c}{24\pi} \left( \frac{2\pi}{\beta} \right)^2 + E_{\text{Shock}} \, \delta\left(x^+ - x_0^+\right), \\ \langle \Psi | T_{--}(x^-) | \Psi \rangle &= \frac{c}{24\pi} \left( \frac{2\pi}{\beta} \right)^2 + E_{\text{Shock}} \, \delta\left(x^- - x_0^-\right) \end{aligned} \tag{29}$$

in the $\varepsilon \to 0$ limit. The coefficient of the delta functions is related to the conformal dimension $\Delta$ of this local operator:

$$E_{\text{Shock}} = \frac{\Delta}{\varepsilon}. \tag{30}$$

Therefore, the insertion of a local operator creates a pair of shock waves in the black hole geometry; one is left-moving and the other is right-moving. The existence of these shocks is manifested by the delta functional peaks of the CFT stress–energy tensor expectation value. For simplicity, we write $E \equiv E_{\text{Shock}}$ below.

### 4.1 *Dilaton part*

Let us discuss in detail how the shock wave changes the dilaton $\Phi$. It satisfies the following equations of motion:

$$-e^{2\omega}\partial_{\pm}\left(e^{-2\omega}\partial_{\pm}\Phi\right) = 2X_{\beta} + E\,\delta\left(x^{\pm} - x_0^{\pm}\right),$$
$$\partial_{+}\partial_{-}\Phi = \frac{\Lambda}{4}e^{2\omega}. \tag{31}$$

These equations are obtained by substituting the stress tensor expectation value (29) into Eq. (12) for arbitrary $\langle T_{\pm\pm}\rangle$. By solving these equations, we obtain the dilaton profile in the presence of the shock wave:

$$\Phi = \phi_0 + \frac{\Lambda}{4}\tan x^{+}\tan x^{-} - X_{\beta}\left(x^{+}\tan x^{+} + x^{-}\tan x^{-}\right) - E\cos^2 x_0^{+}\left(\tan x^{+} - \tan x_0^{+}\right)$$
$$\times\,\theta\left(x^{+} - x_0^{+}\right) - E\cos^2 x_0^{-}\left(\tan x^{-} - \tan x_0^{-}\right)\theta\left(x^{-} - x_0^{-}\right), \tag{32}$$

where $\theta(x)$ is the step function:

$$\theta(x) = \begin{cases} 1 & x > 0 \\ 0 & x < 0. \end{cases} \tag{33}$$

### 4.2 *Classical extremal surfaces*

Now we would like to specify the classical extremal surfaces in the spacetime with the dilaton profile (32). We will see that the actual locations of these surfaces strongly depend on where we insert the local operator. In the right wedge of the local operator $x^{\pm} > x_0^{\pm}$, the dilaton coincides with $\Phi_{\beta,\,E}$ defined by

$$\Phi_{\beta,E} = \phi_0 + \frac{\Lambda}{4}\tan x^{+}\tan x^{-} - X_{\beta}\left(x^{+}\tan x^{+} + x^{-}\tan x^{-}\right)$$
$$- E\cos^2 x_0^{+}\left(\tan x^{+} - \tan x_0^{+}\right) - E\cos^2 x_0^{-}\left(\tan x^{-} - \tan x_0^{-}\right). \tag{34}$$

In the left wedge $x^{\pm} < x_0^{\pm}$, it agrees with with the original profile $\Phi = \Phi_{\beta,\,E=0} \equiv \Phi_{\beta}$ (15); see Fig. 6. We also argued that in the absence of the shock wave, i.e., $E = 0$, the black hole has a causal shadow region in its interior, so it has two bifurcation surfaces. In the presence of the shock, the dilaton profile (32) also has two critical points, one near the left spatial infinity $(x^{+}, x^{-}) = (-\frac{\pi}{2}, -\frac{\pi}{2})$ and the other near the right spatial infinity $(x^{+}, x^{-}) = (\frac{\pi}{2}, \frac{\pi}{2})$. In this section, we only consider the operator insertions, which do not change the location of the left horizon of the undeformed dilaton $\Phi_{\beta}$. This is equivalent to restricting the range of the insertion to $0 < x_0^{+} + x_0^{-}$. Under this restriction, we can focus on the change of the location of the right critical point below. A similar discussion for operator insertions in the $x_0^{+} + x_0^{-} < 0$ region can be had.

To identify the right extremal surface, it is convenient to introduce two characteristic points of the dilaton profile $\Phi$. First, let $x^{\pm} = x_H^{\pm}(0)$ be the critical point of the original dilaton profile $\Phi_{\beta}(x^{\pm})$, i.e.,

$$\partial_{\pm}\Phi_{\beta}|_{x^{\pm}=x_H^{\pm}(0)} = 0 \to \tan\, x_H^{\pm}(0) = \frac{2\pi}{\Lambda}X_{\beta}. \tag{35}$$

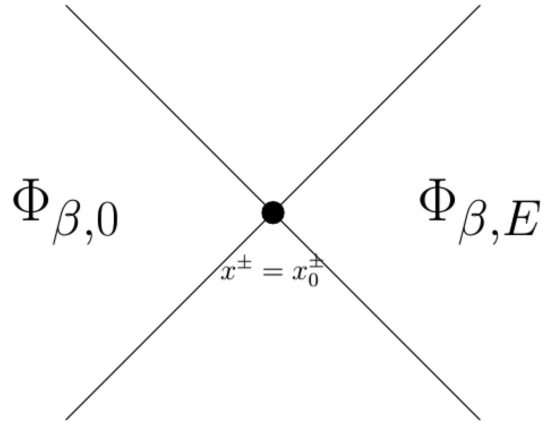


**Fig. 6.** The dilaton profile (32) in the presence of the shock wave. In the right wedge of the local operator, $x^{\pm} > x_0^{\pm}$, we have $\Phi = \Phi_{\beta,\,E}$ with Eq. (34). On the left wedge, $x^{\pm} < x_0^{\pm}$, the dilaton profile coincides with $\Phi_{\beta,\,0}$, which is identical to Eq. (15).

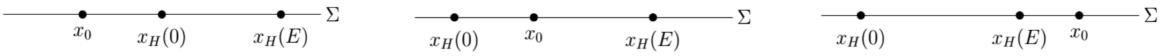


**Fig. 7.** Three possible locations of the local operator $\mathcal{O}$ on the reflection symmetric slice $\Sigma$: $x^+ = x^-$. Left: When $x_0 < x_H(0) < x_H(E)$, the extremal surface is at $x^{\pm} = x_H(E)$. Middle: When $x_H(0) < x_0 < x_H(E)$, both $x^{\pm} = x_H(0)$ and $x^{\pm} = x_H(E)$ are extremal. Right: When $x_H(0) < x_H(E) < x_0$, the extremal surface is at $x^{\pm} = x_H(0)$.

The second characteristic point is $x^{\pm} = x_H^{\pm}(E)$, which is the critical point of the deformed dilaton profile $\Phi_{\beta,\,E}$ (34). It satisfies

$$\tan\, x_H^{\pm}(E) = \frac{4}{\Lambda}\left(\frac{\pi}{2}X_\beta + E\cos^2 x_0\right). \tag{36}$$

These are candidates of the extremal surfaces of the total dilaton (32), but whether these are the critical points of the actual dilaton (32) depends on the location of the local operator $x^{\pm} = x_0^{\pm}$.

In order to simplify the discussion below, instead of exhausting all possible cases, let us first consider the symmetric insertions $x_0^+ = x_0^- \equiv x_0$. Now these two candidate extremal surfaces are also symmetric, i.e., they are on the reflection symmetric slice: $x_H^+(0) = x_H^-(0) \equiv x_H(0)$ and $x_H^+(E) = x_H^-(E) \equiv x_H(E)$. In general, the relation $x_H(0) < x_H(E)$ holds. In this setup, there are three distinct cases for the operator insertions (see Fig. 6). Namely, the location of the operator is (1) behind the original horizon $x_0 < x_H(0)$; (2) in the middle of two horizons, $x_H(0) < x_0 < x_H(E)$; and (3) in the exterior of the deformed horizon, $x_H(E) < x_0$.

Case 1: In the first case, the local operator $\mathcal{O}$ is inserted to the left of the original horizon: $x_0 < x_H(0)$ (left panel of Fig. 7). In this case, only the extremal surface is the deformed horizon $x^{\pm} = x_H(E)$. This is because $x^{\pm} = x_H(0)$ is not a critical point of the dilaton profile (32) since around this point this profile coincides with the deformed one $\Phi_{\beta,\,E}$ (34) due to the condition $x_0 < x_H(0)$. The dilaton value at the extremal surface is given by $\Phi(x_H(E)) = \Phi_{\beta,\,E}(x_H(E))$.

Case 2: In the second case, the local operator is inserted in between two would-be extremal surfaces $x_H(0) < x_0 < x_H(E)$ (middle panel of Fig. 7). In this case, both horizons $x^{\pm} = x_H^{\pm}(0)$ and $x^{\pm} = x_H^{\pm}(E)$ are actually extremal surfaces of the dilaton profile (32).

Case 3: In the third case, the local operator is inserted to the right of the deformed horizon $x_H(E) < x_0$ (right panel of Fig. 7). In this case, only the extremal surface is the origi-

nal horizon $x^{\pm} = x^{\pm}_H(0)$. This is again because the deformed horizon $x^{\pm} = x^{\pm}_H(E)$ is not the critical point of the dilaton. The dilaton value at the extremal surface is given by $\Phi_\beta(x^{\pm}_H(0))$.

### 4.3 *CFT entropy part*

The second ingredient of the generalized entropy (26) is the CFT entropy $S_{\beta,E}[\bar{C}]$ of the density matrix (27) on $\bar{C}$ in the gravitating universe $B$. Because we focus on the high-temperature limit $\beta \to 0$, this region is the disjoint union of two pieces $\bar{C} = \bar{C}_1 \cup \bar{C}_2$, as in the previous section. We put the coordinates of $\bar{C}$ as follows:

$$\begin{cases} x_2^{\pm} = -\frac{\pi}{2}, \\ x_3^{\pm} = x_3 \pm t_3, \end{cases} \quad \text{for } \bar{C}_1,$$

$$\begin{cases} x_5^{\pm} = x_5 \pm t_5, \\ x_6^{\pm} = \frac{\pi}{2}, \end{cases} \quad \text{for } \bar{C}_2.$$

In the $\beta \to 0$ limit, $x_3^{\pm} \to x_2^{\pm}$ and $x_5^{\pm} \to x_6^{\pm}$ holds. Therefore, in the absence of the shock wave $E = 0$, the CFT entanglement entropy for $\bar{C} = \bar{C}_1 \cup \bar{C}_2$ at finite temperature $\beta$ is given by

$$\begin{aligned} S_\beta[\bar{C}] = &\frac{c}{6}\log\left[\frac{\beta}{\pi\varepsilon_{\rm UV}}\sinh\left(\frac{\pi}{\beta}\left(x_3^+ - x_2^+\right)\right)\right] + \frac{c}{6}\log\left[\frac{\beta}{\pi\varepsilon_{\rm UV}}\sinh\left(\frac{\pi}{\beta}\left(x_3^- - x_2^-\right)\right)\right] \\ &+ \frac{c}{6}\log\left[\frac{\beta}{\pi\varepsilon_{\rm UV}}\sinh\left(\frac{\pi}{\beta}\left(x_6^+ - x_5^+\right)\right)\right] + \frac{c}{6}\log\left[\frac{\beta}{\pi\varepsilon_{\rm UV}}\sinh\left(\frac{\pi}{\beta}\left(x_6^- - x_5^-\right)\right)\right]. \end{aligned} \tag{37}$$

We also need the CFT entropy for $\bar{C} = \bar{C}_1 \cup \bar{C}_2$ at zero temperature, and it is given by

$$\begin{aligned} S_{\rm vac}[\bar{C}] = &\frac{c}{6}\log\left[\frac{1}{\varepsilon_{UV}}\sin\left(x_3^+ - x_2^+\right)\right] + \frac{c}{6}\log\left[\frac{1}{\varepsilon_{UV}}\sin\left(x_3^- - x_2^-\right)\right] \\ &+ \frac{c}{6}\log\left[\frac{1}{\varepsilon_{UV}}\sin\left(x_6^+ - x_5^+\right)\right] + \frac{c}{6}\log\left[\frac{1}{\varepsilon_{UV}}\sin\left(x_6^- - x_5^-\right)\right]. \end{aligned} \tag{38}$$

#### 4.3.1 *CFT entropy for a single interval.*

Next, we discuss the entanglement entropy $S_{\beta,E}[\bar{C}]$ in the presence of a shock wave. This kind of entanglement entropy was studied in Ref. [51], which we review in Appendix A. As a warm-up, let us compute the entanglement entropy $S_{\beta,E}[\bar{C}]$ of the single interval,

$$\bar{C} : x_5^{\pm} < x^{\pm} < x_6^{\pm} = \frac{\pi}{2}, \tag{39}$$

which ends at the asymptotic infinity $x_6^{\pm} = \frac{\pi}{2}$. In presenting the expression of the CFT entropy, it is convenient to first fix the subsystem $\bar{C}$, i.e., fixing $x_5^{\pm}$.

This entanglement entropy can be computed by first writing the Rényi entropy $\mathrm{tr}\rho_{\bar{C}}^n$ by a four-point function involving twist operators,

$$\mathrm{tr}\rho_{\bar{C}}^n = \mathrm{tr}\left[\rho_\beta\ \mathcal{O}^{\otimes n}(x_1)\sigma_n(x_5)\sigma_{-n}(x_6)\mathcal{O}^{\otimes n}(x_4)\right], \tag{40}$$

and taking the $n \to 1$ limit of the correlator. Here $x_1$ and $x_4$ are related to $x_0$ through Eq. (A4). When the central charge of the theory is large $c \gg 1$ and its spectrum is sparse, the right-hand side can be approximated by the vacuum conformal block with a choice of branch [51]. Again, details can be found in the appendix.

The possible form of the CFT entropy is constrained by the causal relation between the location of the operator $x^{\pm} = x_0^{\pm}$ and the region $\bar{C}$ [47–57,63]. Indeed, the insertion creates

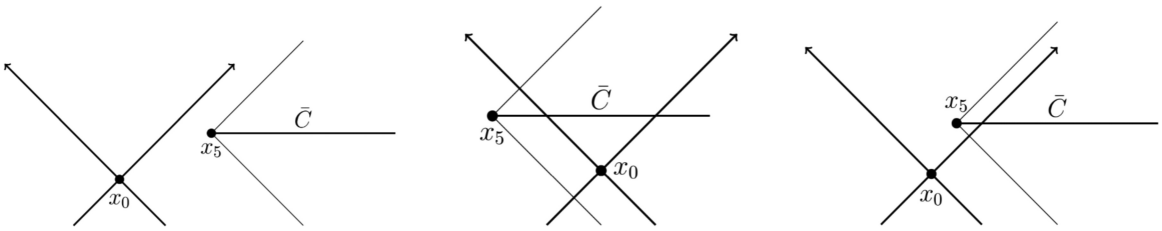


**Fig. 8.** Three possible causal relations between the operator at $x^{\pm} = x_0^{\pm}$ and the interval $\bar{C}$. Left and middle: The local operator is spatially separated from $\bar{C}$. In this case, the non-trivial part of the CFT entropy $\Delta S$ in the generalized entropy is vanishing due to causality. Right: When the local operator and $\bar{C}$ are causally connected, the right-mover emitted by the quench can enter the causal diamond of $D[\bar{C}]$. In this case only, $\Delta S$ is non-vanishing.

shock waves, both left-moving and right-moving, which are roughly speaking interpreted as an entangled pair of particles. Then the CFT entropy can be non-trivial only when one of these shock waves enters the causal diamond of the region $D[\bar{C}]$, whereas its partner does not. Therefore, for the fixed end point of the subsystem, $x^{\pm} = x_5^{\pm}$, we have four possible behaviors of the entropy, according to the location of the local operator relative to the end point as in Fig. 8.

(1) When the end point $x_5$ is in the right wedge of the location of the operator $x_0$, i.e., $x_5^{\pm} > x_0^{\pm}$, neither left-mover nor right-mover enter the causal diamond $D[\bar{C}]$ of the subsystem $\bar{C}$. Therefore, the shock wave cannot affect the state on the subsystem $\bar{C}$, the entanglement entropy remains unchanged due to causality.
(2) Similarly, when the end point is in the left wedge of the insertion $x_0^{\pm} > x_5^{\pm}$, both shock waves enter the causal diamond, and the entanglement entropy again remains unchanged.
(3) When the local operator is in the future or past of the end point, the entanglement entropy can be non-trivial. When it is in the future light cone of the end point $x_5$, i.e., $x_5^- > x_0^-$ and $x_0^+ > x_5^+$, then only the left-moving shock contributes to the entropy. The difference between this entanglement entropy and the thermal one $\Delta S \equiv S_{\beta,E}[\bar{C}] - S_{\beta}[\bar{C}]$ is given by [51]

$$\Delta S_F = \frac{c}{6} \log \left[ \frac{\beta}{\pi \varepsilon} \frac{\sin \pi\alpha}{\alpha} \frac{\sinh \frac{\pi}{\beta}\left(x_0^+ - x_5^+\right) \sinh \frac{\pi}{\beta}\left(x_6^+ - x_0^+\right)}{\sinh \frac{\pi}{\beta}\left(x_6^+ - x_5^+\right)} \right]. \tag{41}$$

When the operator is in the past light cone of the end point, $x_0^- > x_5^-$ and $x_5^+ > x_0^+$, then only the right-mover contributes, and the entropy difference is

$$\Delta S_P = \frac{c}{6} \log \left[ \frac{\beta}{\pi \varepsilon} \frac{\sin \pi\alpha}{\alpha} \frac{\sinh \frac{\pi}{\beta}\left(x_0^- - x_5^-\right) \sinh \frac{\pi}{\beta}\left(x_6^- - x_0^-\right)}{\sinh \frac{\pi}{\beta}\left(x_6^- - x_5^-\right)} \right]. \tag{42}$$

4.3.2 *CFT entropy for two disjoint intervals.* In the actual calculations of the generalized entropy, we need an expression of the CFT entanglement entropy for two disjoint intervals $\bar{C} = \bar{C}_1 \cup \bar{C}_2$. Again, the behavior of the entanglement entropy is strongly constrained by causality. In the previous section, we saw that these two intervals become smaller and smaller $\bar{C}_1,\ \bar{C}_2 \to 0$ in the high-temperature limit $\beta \to 0$. This means that the entropy of these two disjoint intervals

gets factorized,

$$S[\bar{C}] = S[\bar{C}_1] + S[\bar{C}_2], \tag{43}$$

so the result for the single interval is enough to fix the generalized entropy in this limit. For simplicity, we assume that the shock wave does not intersect the left interval $\bar{C}_1$, i.e., $x_0^{\pm}$, so only the entropy of the right interval $S[\bar{C}_2]$ can change non-trivially.

### 4.4 *Quantum extremal surfaces*

We are interested in how the dominant quantum extremal surface changes as we tune the location of the operator $x_0$. We are especially interested in the high-temperature limit $\beta \to 0$, where the classical horizon is getting close to infinity $x^{\pm} = \frac{\pi}{2}$. It is convenient to decompose the CFT entropy $S_{\beta,E}[\bar{C}] - S_{\text{vac}}[\bar{C}]$ in Eq. (26) into a trivial part $S_{\beta}[\bar{C}] - S_{\text{vac}}[\bar{C}]$, which does not involve a shock wave, and a non-trivial part $\Delta S = S_{\beta,E}[\bar{C}] - S_{\beta}[\bar{C}]$. Then the trivial part does not play any role in the generalized entropy in the high-temperature limit. As we saw in the previous section, the classical extremal surfaces in this limit are given by the bifurcation surfaces of the black hole. Therefore, we can focus on the non-trivial part of the CFT entropy to find the quantum extremal surfaces. Without going into detail, let us describe two limiting cases.

First, when the insertion is made in the deep interior of the black hole $x_0 \sim 0$, the true quantum extremal surface almost coincides with the classical horizon of the deformed black hole (the one with back-reaction of the shock wave) at $x^{\pm} = x_H^{\pm}(E)$, defined in Eq. (36). This is because the local operator is spatially separated from the horizon, so the non-trivial part of the CFT entropy $\Delta S$ is vanishing due to causality.

On the other hand, if the operator is inserted at the exterior of the horizon, i.e., $x_0 > x_H(E)$, then, since again the non-trivial part of the CFT entropy is vanishing, the QES coincides with the classical extremal surface, which is identified with the horizon of the original black hole (i.e., the black hole without the shock wave) at $x^{\pm} = x_H^{\pm}(0)$ (35). Below, we discuss the details of the dynamics of QESs.

We remark that the generalized entropies also have a contribution from the left classical extremal surface, which is independent of the location of the operator as long as the operator is inserted at the region $x_0^+ + x_0^- > 0$. The contribution from the left extremal surface is given by Eq. (22) in the high-temperature limit; let us denote it by $S_L$. Then, the generalized entropies for each case are given as follows.

Case 1: When the local operator is inserted inside of the original horizon (the left panel of Fig. 8), $x_0 < x_H(0)$, the quantum extremal surface coincides with the bifurcation surface of the deformed black hole at $x^{\pm} = x_H(E)$. Also, since $\Delta S = 0$ in this case, we get the following expression for the generalized entropy:

$$\begin{aligned} S_{\text{gen}} &= \Phi_{\beta,E}(x_H(E)) + S_L \\ &= \phi_0 - \frac{4}{\Lambda}\left[\left(\frac{\pi X_\beta}{2}\right)^2 + \pi X_\beta E \cos^2 x_0\right] \\ &\quad - \frac{4}{\Lambda}E^2 \cos^4 x_0 + 2E \cos^2 x_0 \tan x_0 + S_L. \end{aligned} \tag{44}$$

Case 2: When we insert the operator in between two bifurcation surfaces (the middle panel of Fig. 8), $x_H(0) < x_0 < x_H(E)$, the generalized entropy is given by

$$\begin{aligned} S_{\text{gen}} &= \min\left\{\Phi_\beta(x_H(0)),\ \Phi_{\beta,E}(x_H(E))\right\} + S_L \\ &= \phi_0 - \frac{(\pi X_\beta)^2}{\Lambda} \\ &\quad + \min\left\{0, -2E\cos^2 x_0\left(\frac{2\pi X_\beta}{\Lambda} + \frac{2}{\Lambda}E\cos^2 x_0 - \tan x_0\right)\right\} + S_L. \end{aligned} \tag{45}$$

Again in this case the non-trivial part of the CFT entropy $\Delta S$ vanishes.

The transition point $x^\pm = x_T$, at which the dominance in the minimization of the above expression changes, satisfies the equation

$$\tan x_T = \frac{2\pi X_\beta}{\Lambda} + \frac{2}{\Lambda}E\cos^2 x_T. \tag{46}$$

Case 3: When the operator is inserted at the outside of the deformed horizon (the right panel of Fig. 8), $x_H(E) < x_0$, we have

$$\begin{aligned} S_{\text{gen}} &= \Phi_\beta\left(x_H(0)\right) + S_L \\ &= \phi_0 - \frac{(\pi X_\beta)^2}{\Lambda} + S_L. \end{aligned} \tag{47}$$

Net result: By combining the above results, we get the generalized entropy in the high-temperature limit as a function of $x_0$:

$$S_{\text{gen}}\ (x_0) = \begin{cases} \phi_0 - \frac{(\pi X_\beta)^2}{\Lambda} - 2E\cos^2 x_0\left(\frac{2\pi X_\beta}{\Lambda} + \frac{2}{\Lambda}E\cos^2 x_0 - \tan x_0\right) \\ \qquad + S_L \qquad \text{for } x_0 < x_T \\ \phi_0 - \frac{(\pi X_\beta)^2}{\Lambda} + S_L \qquad \text{for } x_T < x_0. \end{cases} \tag{48}$$

We plot the above generalized entropy for several values of $E$ in Fig. 9.[3]

From the plot we see that, when the operator is in the exterior of the horizon, the generalized entropy does not change. On the other hand, when it is inserted in the black hole interior it always make the entropy decrease. Also, we observe that, as the location of the local operator goes deeper into the interior of the black hole, the entropy decreases significantly. This is because, if the shock wave is created inside of the horizon, it makes the interior wormhole region longer (which is seen from the relation $x_H(0) < x_H(E)$) and reduces the entropy of the black hole $\Phi_\beta(x_H(0)) > \Phi_{\beta,E}(x_H(E))$. Therefore, in some sense what the shock wave does is to make the black hole further "evaporate". This black hole in universe $B$ has been evaporating due to the entanglement with the non-gravitating universe $A$, and the insertion of the local operator accelerates the evaporation, which leads to the faster decrease of the entropy.

The actual entanglement entropy $S(\rho_A)$ is given by the minimum between $S_{\text{no-island}}$ and $S_{\text{gen}}(x_0)$. We plot this curve in Fig. 10. Since we are interested in how this $S(\rho_A)$ changes as we increase the entanglement temperature $1/\beta$, we plot it as a function of $1/\beta$ while the location of the operator $x^\pm = x_0^\pm$ is kept fixed. As we increase the entanglement temperature, the bifurcation surface of the black hole approaches the asymptotic infinity, and the operator at

[3]The plots shown in this paper are obtained by full numerical calculations by faithfully extremizing the generalized entropies, in contrast to the analytical expressions appearing in the body of the paper.

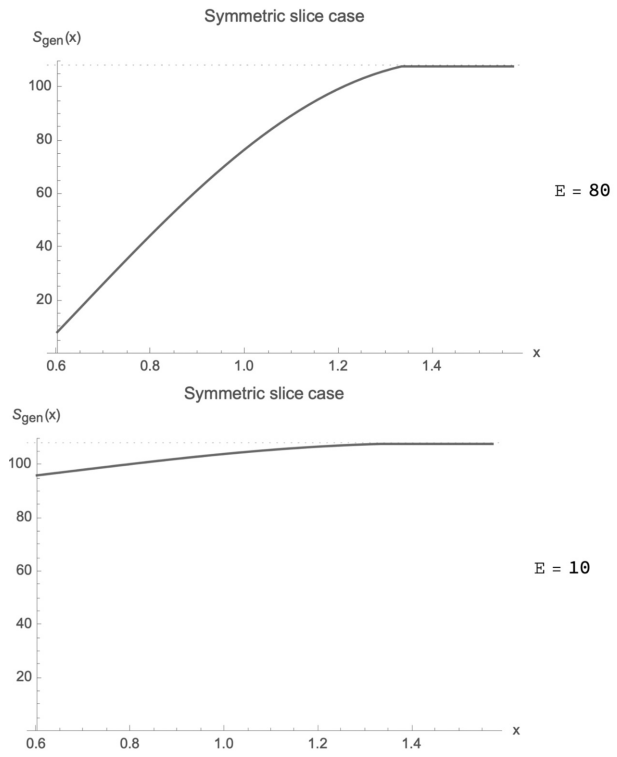


**Fig. 9.** Plots of $S_{\rm gen}$ (48) as a function of $x_0$ ($0 \leq x_0 \leq \pi/2$) with $\phi_0 = 1700,\ \beta = 1,\ \Lambda = 500,\ c = 50,\ \varepsilon = 0.1.\ \Delta = 8\,(E = 80)$ (top) and $\Delta = 1\,(E = 10)$ (bottom). The dotted line is the value of the entropy for the shockless case, $\Delta = 0\,(E = 0)$.

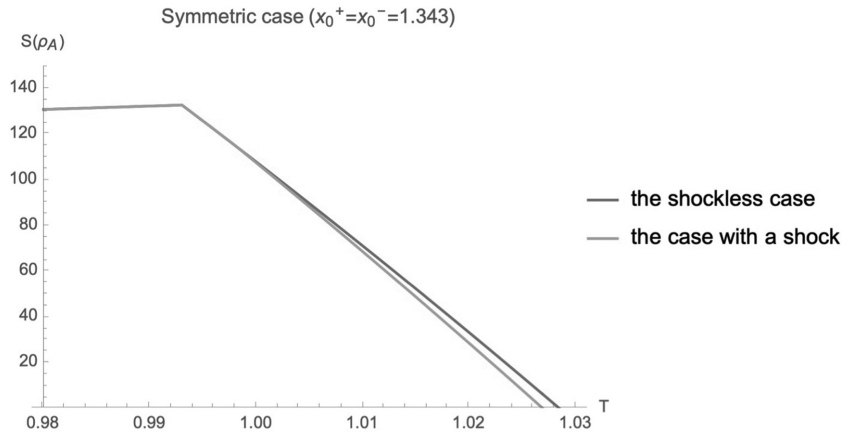


**Fig. 10.** Plots of the Page curves corresponding to the shockless case (24) and the case with a shock (49) as a function of $T = 1/\beta$ with fixing the position of the operator, which we place on the reflection symmetric slice $x_0^+ = x_0^-$. $\phi_0 = 1700,\ \Lambda = 500,\ c = 50,\ \Delta = 10,\ \varepsilon = 0.01,\ x_0^+ = x_0^- = 1.343$. The island begins dominating at $T \simeq 0.993$ and the location of the corresponding QES is $x_H^+(0) = x_H^-(0) \simeq 1.328$. The entanglement entropy with a shock decreases faster than the one without it.

$x^\pm = x_0^\pm$ is eventually absorbed into the black hole. We again observe that, above some critical temperature, the entanglement entropy is dominated by the generalized entropy $S_{\rm gen}(x_0)$ (48). In the high-temperature limit, since the operator goes into the deep interior of the black hole, $S_{\rm gen}(x_0)$ is given by the first line of Eq. (48). Therefore an approximate expression for the

entanglement entropy reads:

$$S(\rho_A) = \begin{cases} S_{\text{no-island}} = \frac{\pi^2 c}{3\beta} & \beta \gg \beta_c \\ S_{\text{gen}}(x_0) = \phi_0 - \frac{(\pi X_\beta)^2}{\Lambda} - 2E\cos^2 x_0 \left( \frac{2\pi X_\beta}{\Lambda} + \frac{2}{\Lambda} E\cos^2 x_0 - \tan x_0 \right) + S_L & \beta \ll \beta_c. \end{cases} \tag{49}$$

It is interesting to compare this result with the Page curve without the operator insertion (24). In this case, above the critical temperature the entropy decreases as

$$S_{\text{island}} = \phi_0 - \frac{(\pi X_\beta)^2}{\Lambda} + S_L. \tag{50}$$

By comparing this with Eq. (49), we see that the entropy in the presence of the shock wave is reduced faster than the entropy without the shock, by increasing the entanglement temperature. This also supports the point of view that the shock wave accelerates the evaporation of the black hole.

### 4.5 *QESs with non-trivial CFT entropy*

In the above examples, the CFT entropy did not play any role. This is because, when the operator is inserted in the time reflection symmetric slice $x_0^+ = x_0^-$, the quantum extremal surfaces and the local operator are always spatially separated; therefore the non-trivial part of the CFT entropy $\Delta S = S_{\beta,E}[\bar{C}] - S_\beta[\bar{C}]$ vanishes in the generalized entropy. As a result, the QESs coincide with the classical extremal surfaces, which can be identified with the bifurcation surfaces of the black hole. On the other hand, when we insert the operator in the future light cone of the original horizon $x^\pm = x_H^\pm(0)$, then the non-trivial part of the CFT entropy is non-vanishing. In this case, we insert the local operator in the region $x_0^+ > x_H^+(0)$, $x_0^- < x_H^-(0)$. Let us first derive the location of the classical extremal surface. The dilaton profile is still given by Eq. (32), and since we expect that the new bifurcation surface is in the past light cone of the operator, we extremize

$$\begin{aligned} \Phi_R\left(x^\pm\right) = \phi_0 + \frac{\Lambda}{4}\tan x^+ \tan x^- - X_\beta\left(x^+\tan x^+ + x^-\tan x^-\right) \\ - E\cos^2 x_0^-\left(\tan x^- - \tan x_0^-\right). \end{aligned} \tag{51}$$

The critical point $(x_{\mathcal{H}}^+(E), x_{\mathcal{H}}^-(E))$ of this dilaton profile $\Phi_R(x^\pm)$ satisfies

$$x_{\mathcal{H}}^-(E) = x_H^-(0), \quad \tan x_{\mathcal{H}}^+(E) = \tan x_H^+(0) + \frac{4E}{\Lambda}\cos^2 x_0^-. \tag{52}$$

We remark that this is different from the critical point $(x_H^+(E), x_H^-(E))$ of $\Phi_{\beta,E}$ (34) discussed in the previous subsection.

The net effect of the shock wave is to shift the horizon along the $x^+$ direction. In order for this critical point $(x_{\mathcal{H}}^+(E), x_{\mathcal{H}}^-(E))$ to be really in the past light cone of the operator, we need

$$\tan x_H^+(0) + \frac{4E}{\Lambda}\cos^2 x_0^- < \tan x_0^+. \tag{53}$$

Now let us add quantum effects. The expression of the generalized entropy can be obtained from Eq. (41):

$$\begin{aligned} S_{\text{gen}}\left(x^\pm\right) = \Phi_R\left(x^\pm\right) + \frac{c}{6}\log\left[\frac{\beta}{\pi\varepsilon}\frac{\sin\pi\alpha}{\alpha}\frac{\sinh\frac{\pi}{\beta}\left(x_0^+ - x_5^+\right)\sinh\frac{\pi}{\beta}\left(x_6^+ - x_0^+\right)}{\sinh\frac{\pi}{\beta}\left(x_6^+ - x_5^+\right)}\right] \\ + S_\beta[\bar{C}] - S_{\text{vac}}[\bar{C}] + S_L, \end{aligned} \tag{54}$$

where $S_L$ is the contribution of the left horizon, as in the previous subsection. In the high-temperature limit, $S_L = \Phi_\beta(x_H^\pm(0))$, defined in Eq. (22).

We then specify the location of the quantum extremal surface $x^\pm = x_{Q_1}^\pm$ by finding the critical point of the above generalized entropy (54). Since its derivative along the $x^-$ direction is not affected by the non-trivial part of the CFT entropy $\Delta S$, $\tan x_{Q_1}^+$ is still given by

$$\tan x_{Q_1}^+ = \tan x_H^+(0) + \frac{4E}{\Lambda}\cos^2 x_0^-. \tag{55}$$

The derivative along the $x^+$ direction is modified by $\Delta S$. By ignoring its trivial part $S_\beta[\bar{C}] - S_{\rm vac}[\bar{C}]$, we get

$$\tan x_{Q_1}^- = \frac{4}{\Lambda}\left[\frac{\pi}{2}X_\beta + \frac{c\pi}{6\beta}\cos^2 x_{Q_1}^+\left(\frac{1}{\sinh\frac{\pi}{\beta}\left(x_0^+ - x_{Q_1}^+\right)} - \frac{1}{\sinh\frac{\pi}{\beta}\left(x_6^+ - x_{Q_1}^+\right)}\right)\right]. \tag{56}$$

The contribution of this quantum extremal surface is given by plugging the solutions of Eqs. (55) and (56) into the expression of the generalized entropy (54).

There is another quantum extremal surface, $x^\pm = x_{Q_2}^\pm$ located at the right wedge of the operator $x_{Q_2}^\pm > x_0^\pm$. In this case, the non-trivial part of the CFT entropy $\Delta S$ is vanishing, so it coincides with the bifurcation surface of the original black hole $x_{Q_2}^\pm = x_H^\pm(0)$.

Although we have two candidates for the quantum extremal surface at $x^\pm = x_{Q_1}^\pm$ and $x^\pm = x_{Q_2}^\pm$, they cannot appear simultaneously. This is due to the non-symmetric insertion of the local operator. If we put the local operator in the future light cone of the bifurcation surface of the original black hole $x_0^+ > x_H^+(0)$, $x_0^- < x_H^-(0)$, then the bifurcation surface is moved to $(x_{\mathcal{H}}^+(E), x_{\mathcal{H}}^-(E))$. In this case $x_H^\pm(0) = x_{Q_2}^\pm$ is no longer extremal, and only $x^\pm = x_{Q_1}^\pm$ is the quantum extremal surface. On the other hand, if the operator $x_0^\pm$ is in the exterior of the horizon $x_0^\pm > x_H^\pm(0)$, then only $x^\pm = x_{Q_2}^\pm$ is the quantum extremal surface. Thereby, the generalized entropy is given by

$$S_{{\rm gen},E}\left(x_0^+, x_0^-\right) = \begin{cases} S_{\rm gen}\left(x_{Q_1}^\pm\right) & \text{for} \quad x_H^-(0) > x_0^- \\ S_{\rm gen}\left(x_{Q_2}^\pm\right) & \text{for} \quad x_H^-(0) < x_0^-. \end{cases} \tag{57}$$

In the high-temperature limit, $S_{\rm gen}(x_{Q_1}^\pm)$ is obtained by plugging the solution of Eq. (56) into Eq. (54). $S_{\rm gen}(x_{Q_2}^\pm)$ coincides with the entropy of the original black hole $\Phi_\beta(x_H^\pm(0))$. The actual entanglement entropy is given by the minimum between this generalized entropy and $S_{\text{no-island}}$:

$$S(\rho_A) = \min\left\{S_{\text{no-island}},\ S_{{\rm gen},E}\right\}. \tag{58}$$

4.5.1 *Plot of the result.* Let us focus on the case where the location of the left-mover $x^+ = x_0^+$ is fixed but the location of the right-mover $x^- = x_0^-$ is varied, as in the right panel of Fig. 11. We also demand $x_0^+ > x_H^+(E)$, so that the location of the operator interpolates between the interior and the exterior of the black hole. We plot the generalized entropy $S_{{\rm gen},E}(x_0^\pm)$ in Fig. 12. By decreasing the value of $x_0^-$, the local operator is falling to the black hole horizon, and we are interested in how the entropy changes as the local operator falls to the horizon and eventually enters the interior.[4]

[4]In studying the Page curve for an evaporating black hole, the setup where an AdS black hole is attached to a non-gravitating heat bath at the asymptotic boundary is often used, e.g., in Refs. [2,58,59]. In such a setup, the local operator itself is inserted in the (non-gravitating) bath region, and the shock wave created by the operator can enter the bulk region. Instead, in our setup, we insert the operator in the gravitating

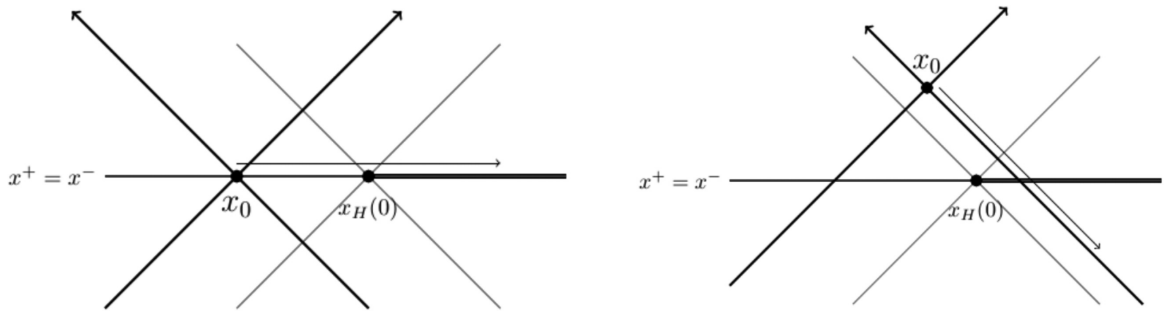


**Fig. 11.** Left: The operator inserted in the time reflection symmetric slice (the blue line). In this case the operator is spatially separated from the bifurcation surface of the black hole at $x^{\pm} = x_H^{\pm}(0)$. (The black hole horizon is shown by the red lines.) Right: The operator inserted in the non-time reflection symmetric slice. In this case, the bifurcation surface can causally contact the operator.

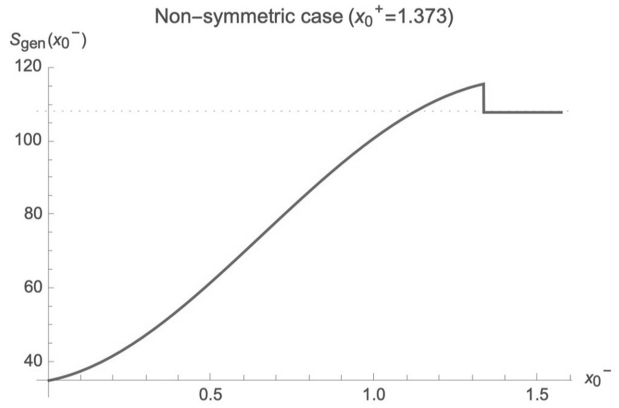


**Fig. 12.** Plot of the generalized entropy given in Eq. (57) as a function of $x_0^-$ with $x_0^+$ kept fixed (the case of the non-symmetric insertion), with the choice of parameters $\phi_0 = 1700$, $\Lambda = 500$, $c = 50$, $\beta = 1$, $\Delta = 7$, $\varepsilon = 0.1$, $x_0^+ = 1.373$. The dotted line corresponds to the shockless case $\Delta = 0$.

The plot in Fig. 12 for the asymmetric insertion is compared to the similar plot shown in Fig. 9, where we insert the operator on the time reflection symmetric slice (48), as in the left panel of Fig. 11. These two plots share a common feature. Namely, when the operator is inserted outside of the horizon $x^- > x_H^-(0)$, the values of these two entropies both approach the classical entropy of the original black hole $\Phi_\beta(x_H^{\pm}(0))$, defined in Eq. (22). This happens because the non-trivial part of the CFT entropy $\Delta S$ vanishes since the local operator is in the causal diamond of $\bar{C}$.

However, these two generalized entropies behave differently when the operator is inserted in the black hole interior $x_0^- < x_H^-(0)$. In particular, there is a bump in the entropy plot for the asymmetric insertion in Fig. 12, which is absent in the plot for the symmetric insertion (Fig. 9). This difference is a direct consequence of the fact that the quantum extremal surface for the asymmetric insertion is in the past of the local operator, so the non-trivial part of the CFT entropy $\Delta S$ is non-vanishing. On the other hand, in the case of the symmetric insertion, the QES is spatially separated from the local operator, so $\Delta S$ is vanishing.

This bump in Fig. 12 can be understood as a result of the dynamics of the black hole. For this purpose, it is useful to follow the plot backward in the $x_0^-$ direction. By decreasing $x_0^-$, the black

universe, and the operator itself can enter the black hole interior. We regard our shock waves as a kind of "heavy diary"; see, e.g., Refs. [3,58,60].

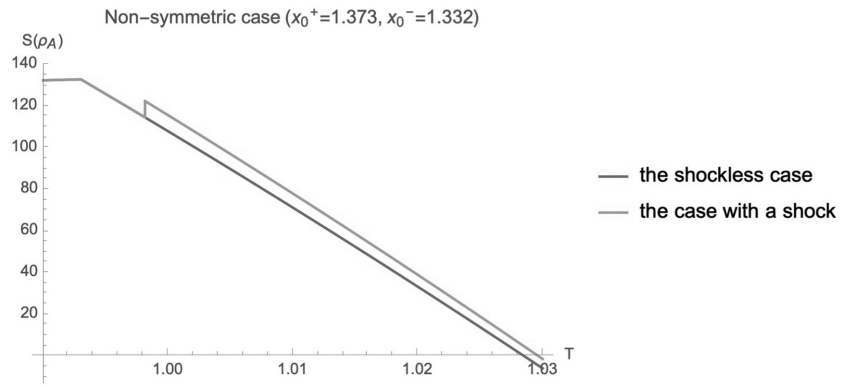


**Fig. 13.** Plots of the Page curves corresponding to the shockless case (24) and the case with a shock wave (58) as a function of $T = 1/\beta$ with fixing the position of the operator, which is not on the reflection symmetric slice, i.e., $x_0^+ \neq x_0^-$, with the choice of parameters $\phi_0 = 1700,\ \Lambda = 500,\ c = 50,\ \Delta = 7,\ \varepsilon = 0.1,\ x_0^+ = 1.373,\ x_0^- = 1.332$. The island begins dominating at $T \simeq 0.993$ and the location of the corresponding QES is $x_H^+(0) = x_H^-(0) \simeq 1.328$.

hole gets bigger due to its absorption of the local operator, and this causes the sudden increase in the entropy in the plot. After the increase in its size, the black hole starts to evaporate again, and as a result the generalized entropy starts decreasing.

One can characterize the difference between these two generalized entropies by the difference in the natures of these two insertions. The symmetric insertion can be regarded as a local operation, because in this case the local operator is always in either the causal diamond of the island $D[C]$ (which can be regarded as part of the radiation system) or the entanglement wedge of the black hole $D[\bar{C}]$, as in the left panel of Fig. 11. Since they are LOCCs, they can only decrease the entanglement entropy. On the other hand, operators inserted asymmetrically enter a region of the black hole interior that belongs to neither of these two entanglement wedges (the right panel of Fig. 11). Therefore, these insertions are not LOCCs, so they can increase the entanglement between the two wedges.

### 4.6 *The entanglement entropy*

The entanglement entropy $S(\rho_A)$ is given by putting these results into the formula (58). Again we plot this as a function of the entanglement temperature $1/\beta$ with the location of the operator $x^\pm = x_0^\pm$ kept fixed in Figs 13 and 14. As we increase the temperature, the horizon expands and the local operator is absorbed into the black hole. So in this case too we can see the identical physics that leads to the result obtained by varying $x_0^-$.

When the location of the operator is properly chosen, the resulting entanglement entropy behaves in a complicated manner as in Fig. 14. This is compared to the same entropy without the shock wave (24), where the transition between $S_{\text{no-island}}$ and $S_{\text{island}}$ happens only once. Instead, in the presence of the shock, the transition can happen multiple times. In the actual plot in Fig. 14, we observe that, at sufficiently low temperatures, $S_{\text{no-island}}$ dominates, and by increasing the entanglement temperature $S_{\text{island}}$ becomes dominant, as we can also see in the case without the shock wave. However, this is not the end of the story. Namely, a further increase in the temperature makes the horizon expand, so the local operator falls to the horizon. This will lead to a size change of the black hole and to a sudden increase of $S_{\text{island}}$. Now this $S_{\text{island}}$ gets larger than the naive Hawking's entropy, so above this temperature $S_{\text{no-island}}$ again dominates.

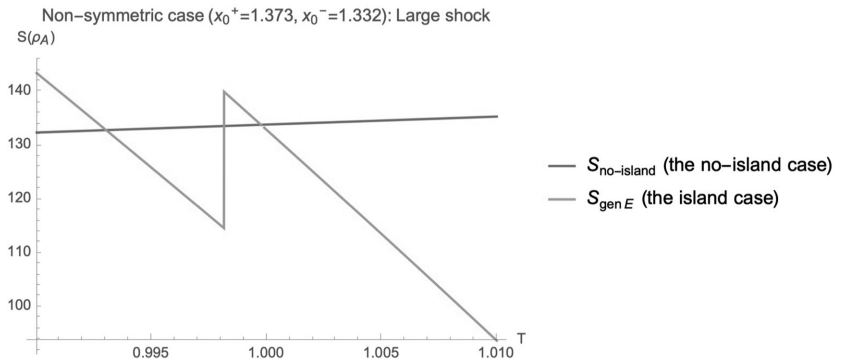


**Fig. 14.** Similar plot to Fig. 13 but the shock wave has a larger energy than the previous case. We plot the Page curve only around the points at which the non-trivial dominance changes happen, unlike the previous case (Fig. 13). The Page curve is given by the minimum of them. We set the parameters to $\phi_0 = 1700,\ \Lambda = 500,\ c = 50,\ \Delta = 8,\ \varepsilon = 0.01,\ x_0^+ = 1.373,\ x_0^- = 1.332$. In this case, the transitions between them happen several times. The first transition is at $T \simeq 0.993$ and the location of the corresponding QES is $x_H^+(0) = x_H^-(0) \simeq 1.328$.

After this, the size of the black hole is eventually reduced due to the emission of Hawking quanta, so eventually $S_{\text{island}}$ gets smaller than $S_{\text{no-island}}$ and becomes dominant once again.

## 5. Conclusion

In this paper, we have studied the dynamics of black holes in flat space when it is entangled with an auxiliary non-gravitating universe. We find that the back-reaction of the entanglement between them reduces the horizon area of the black hole and lengthens its interior region. This lengthening can be understood in terms of the monogamy property of entanglement [28]. Since the gravitating universe $B$ contains two horizons, the Hilbert space of $B$ can be naturally decomposed into two horizon Hilbert spaces $H_{B_L} \otimes H_{B_R}$. Since both of these degrees of freedom are strongly entangled with $H_A$, the entanglement between the two horizons should be suppressed, according to the monogamy of entanglement. This suppression is geometrized by the long interior region of the black hole. We then computed the entanglement entropy between the two universes, and found a Page curve for an evaporating black hole.

We also the studied actions of local operations on the black hole. Such a local operation is modeled by the insertion of a CFT operator. In our setup, it is natural to consider the insertions in the black hole interior in addition to those in the exterior. This insertion can back-react to the black hole through its stress–energy tensor. The (quantum) extremal surfaces in the back-reacted black hole strongly depend on the location of the insertion. There are several differences between the insertions in the interior and exterior. When the operator is in the exterior of the black hole, it does not change the entanglement entropy. On the other hand, the entropy is significantly reduced when the operator is in the interior. The disruption becomes stronger as the location of the insertion gets deeper into the interior of the black hole.

It would be interesting to study how an observer in the non-gravitating universe $A$ can recover information on shock waves in the black hole interior in the gravitating universe $B$. One way to do so is using the modular flow of the reduced density matrix $\rho_A$. Our setup is especially suitable for this purpose. This is because these two universes can be embedded in the larger Minkowski space, in which $AB$ are both realized as the left and right wedges of the origin. Furthermore, the TFD state on $AB$ is identified with the vacuum of this larger Minkowski space. By focusing

on the code subspace, the modular Hamiltonian of $\rho_A$ is approximated by the CFT vacuum modular Hamiltonian of the CFT on $AC$, $-\log\rho_A = K_{AC}^{\mathrm{CFT}}$, where $C$ is the island region in the gravitating universe $B$ [64]. In a CFT with a large central charge and a sparse spectrum, this modular Hamiltonian is given by the sum of two modular Hamiltonians for single intervals, each of which connects the end points of $A$ and $C$. In 2D CFT, this vacuum modular Hamiltonian has a particularly simple form as an integral of the stress–energy tensor. Since this modular flow is geometric, one can visualize how an operator in the black hole interior gets out of the horizon under the flow.

**Acknowledgements**

T.U. thanks Vijay Balasubramanian, Arjun Kar, and Kotaro Tamaoka for useful discussions in the related projects. T.U. was supported by a JSPS Grant-in-Aid for Young Scientists 19K14716.

## Funding

Open Access funding: SCOAP[3].

## Appendix A. Entanglement entropy and local quench for two disjoint intervals

In this appendix we derive the results presented in Sects. 4.3.1 and 4.3.2 for the CFT entanglement entropy in the presence of a local operator insertion by following the argument of Ref. [51]. We are interested in the state (25) of the total system $AB$ and its reduced density matrix on two disjoint intervals $\bar{C}$ in universe $B$. In the body of this paper, this region $\bar{C}$ is identified with the complement of the island $C$ in universe $B$.

Let $\rho_{\bar{C}}$ denote the reduced density matrix on two disjoint intervals $\bar{C} = \bar{C}_1 \cup \bar{C}_2$, whose end points are given by $x_2^{\pm}$ and $x_3^{\pm}$ ($x_2^{\pm} \le x_3^{\pm}$) for $\bar{C}_1$ and $x_5^{\pm}$ and $x_6^{\pm}$ ($x_3^{\pm} < x_5^{\pm} \le x_6^{\pm}$) for $\bar{C}_2$ respectively (see Fig. A1), i.e., $\rho_{\bar{C}} = \mathrm{tr}_C\,\rho$, where $\rho$ is given by the reduced density matrix of universe

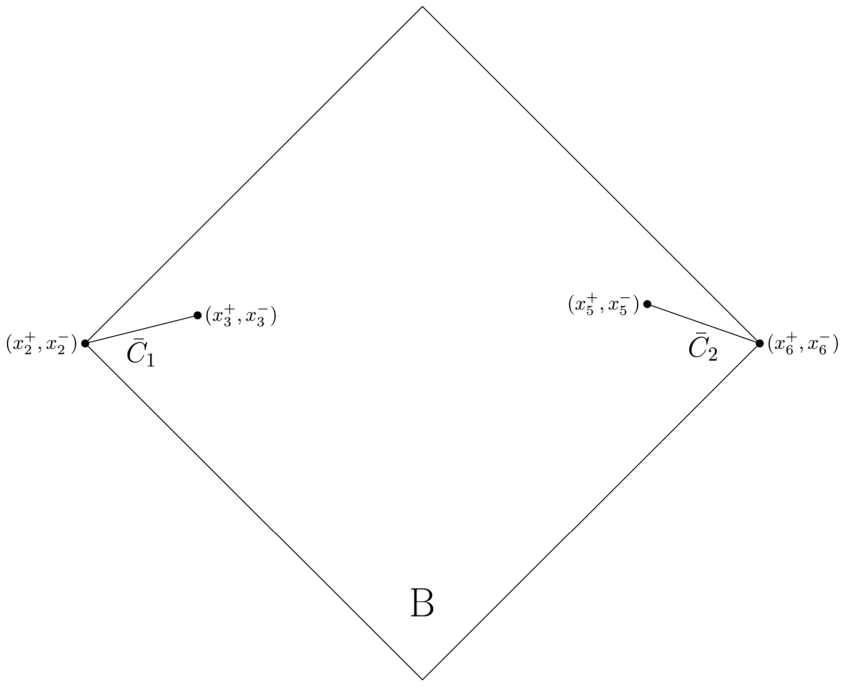


**Fig. A1.** The two intervals in universe $B$.

*B* (27). The CFT entanglement entropy of the density matrix can be calculated by using the replica trick. For this purpose, we first consider the *n*th Rényi entanglement entropy

$$S^{(n)}[\bar{C}] \equiv \frac{1}{1-n} \log \operatorname{tr} \rho_{\bar{C}}^n \tag{A1}$$

and, by taking the limit

$$S[\bar{C}] = \lim_{n \to 1} S^{(n)}[\bar{C}], \tag{A2}$$

we obtain the CFT entanglement entropy.

To evaluate $\operatorname{tr} \rho_{\bar{C}}^n$, we need to compute a normalized $2n$-point function on an $n$-sheeted replica manifold branched along $\bar{C}$. Since the reduced density matrix $\rho_{\bar{C}}$ has a thermal form, each replica sheet is a cylinder with the period $\beta$. This $2n$-point function is identical to the normalized six-point function including twist operators on a (non-replicated) manifold (thermal cylinder) in the cyclic orbifold theory $\mathrm{CFT}^{\otimes n}/Z_n$. We adopt the later description and compute the six-point function

$$\operatorname{tr} \rho_{\bar{C}}^n = \frac{\langle \mathcal{O}^{\otimes n}\left(x_1^+, x_1^-\right) \sigma_n\left(x_2^+, x_2^-\right) \sigma_{-n}\left(x_3^+, x_3^-\right) \sigma_n\left(x_5^+, x_5^-\right) \sigma_{-n}\left(x_6^+, x_6^-\right) \mathcal{O}^{\dagger \otimes n}\left(x_4^+, x_4^-\right)\rangle_\beta}{\left(\langle \mathcal{O}\left(x_1^+, x_1^-\right) \mathcal{O}^\dagger\left(x_4^+, x_4^-\right)\rangle_\beta\right)^n}, \tag{A3}$$

where $\langle \cdots \rangle_\beta$ means the thermal trace $\operatorname{tr}[\rho_\beta \cdots]$.

In the above correlation function, we introduced the UV regulator $\varepsilon$ in the location of the operators as follows:

$$\begin{cases} x_1^\pm = x_0^\pm \mp i\varepsilon, \\ x_4^\pm = x_0^\pm \pm i\varepsilon; \end{cases} \tag{A4}$$

$\mathcal{O}^{\otimes n}$ and $\mathcal{O}^{\dagger \otimes n}$ represent the products of the operators $\mathcal{O}_i$ and $\mathcal{O}_i^\dagger$, which are the $i$th copies of the operators in the cyclic orbifold theory,

$$\begin{aligned} \mathcal{O}^{\otimes n} &= \mathcal{O}_1 \mathcal{O}_2 \cdots \mathcal{O}_n, \\ \mathcal{O}^{\dagger \otimes n} &= \mathcal{O}_1^\dagger \mathcal{O}_2^\dagger \cdots \mathcal{O}_n^\dagger, \end{aligned} \tag{A5}$$

with the conformal dimension $nh_{\mathcal{O}}$; $\sigma_n$ and $\sigma_{-n}$ are twist and anti-twist fields respectively with the conformal dimension $2H_n$:

$$H_n = \frac{c}{24}\left(n - \frac{1}{n}\right). \tag{A6}$$

We will compute the six-point function (A3) in a conformal field theory with gravity dual. Such a CFT has a large central charge and a sparse spectrum. In this class of theories, one can approximate the correlation function by a six-point Virasoro vacuum conformal block with an appropriate choice of branch, following the argument of Ref. [51]. In doing so, it is convenient to map the thermal cylinder to a plane by

$$w^\pm(x^\pm) = \exp\left(\frac{2\pi}{\beta}\left(x^\pm - x_0^\pm\right)\right) \tag{A7}$$

and additionally apply a conformal transformation

$$z^\pm(w^\pm) = \frac{\left(w_1^\pm - w^\pm\right) w_{34}^\pm}{w_{13}^\pm \left(w^\pm - w_4^\pm\right)}, \tag{A8}$$

where we use the notation $w_{ij}^{\pm} = w_i^{\pm} - w_j^{\pm}$. By the conformal map $w^{\pm} \to z^{\pm}$, one can relate $\mathrm{tr}\,\rho_{\bar{C}}^n$ in Eq. (A3) to the correlator on the plane,

$$\begin{aligned}\mathrm{tr}\,\rho_{\bar{C}}^n = &\left(\left(1-z^+\right)\left(1-z^-\right)\right)^{2H_n}\left(z_{65}^+ z_{65}^-\right)^{2H_n}\\ &\times\left\{\left(\frac{\beta}{\pi\varepsilon_{\mathrm{UV}}}\right)^4 \sinh\left(\frac{\pi}{\beta}x_{65}^+\right)\sinh\left(\frac{\pi}{\beta}x_{65}^-\right)\sinh\left(\frac{\pi}{\beta}x_{32}^+\right)\sinh\left(\frac{\pi}{\beta}x_{32}^-\right)\right\}^{-2H_n}\\ &\times\langle\mathcal{O}^{\otimes n}\left|\sigma_n\left(z^+,z^-\right)\sigma_{-n}(1,1)\sigma_n\left(z_5^+,z_5^-\right)\sigma_{-n}\left(z_6^+,z_6^-\right)\right|\mathcal{O}^{\otimes n}\rangle,\end{aligned} \tag{A9}$$

where we introduce the UV cutoff $\varepsilon_{\mathrm{UV}}$ and the notation

$$\begin{aligned}&\langle\mathcal{O}^{\otimes n}\left|\sigma_n\left(z^+,z^-\right)\sigma_{-n}(1,1)\sigma_n\left(z_5^+,z_5^-\right)\sigma_{-n}\left(z_6^+,z_6^-\right)\right|\mathcal{O}^{\otimes n}\rangle\\ &\equiv\lim_{z_4^+,z_4^-\to\infty}\left(z_4^+z_4^-\right)^{2nh_{\mathcal{O}}}\langle\mathcal{O}^{\dagger\otimes n}\left(z_4^+,z_4^-\right)\sigma_n\left(z^+,z^-\right)\sigma_{-n}(1,1)\\ &\quad\times\sigma_n\left(z_5^+,z_5^-\right)\sigma_{-n}\left(z_6^+,z_6^-\right)\mathcal{O}^{\otimes n}(0,0)\rangle.\end{aligned} \tag{A10}$$

Next, we evaluate Eq. (A10) with the insertion of a complete set as follows:

$$\begin{aligned}&\langle\mathcal{O}^{\otimes n}\left|\sigma_n\left(z^+,z^-\right)\sigma_{-n}(1,1)\sigma_n\left(z_5^+,z_5^-\right)\sigma_{-n}\left(z_6^+,z_6^-\right)\right|\mathcal{O}^{\otimes n}\rangle\\ &=\sum_{\alpha}\langle\mathcal{O}^{\otimes n}\left|\sigma_n\left(z^+,z^-\right)\sigma_{-n}(1,1)|\alpha\rangle\langle\alpha|\sigma_n\left(z_5^+,z_5^-\right)\sigma_{-n}\left(z_6^+,z_6^-\right)\right|\mathcal{O}^{\otimes n}\rangle,\end{aligned} \tag{A11}$$

where the sum runs over all possible intermediate states. However, in the $\varepsilon\to 0$ limit, $z^{\pm}$ approach 1, and since the OPE $\sigma_n(z)\sigma_{-n}(1)$ starts from the identity, one can approximate the six-point function as a product of four-point functions,

$$\begin{aligned}&\langle\mathcal{O}^{\otimes n}\left|\sigma_n\left(z^+,z^-\right)\sigma_{-n}(1,1)\sigma_n\left(z_5^+,z_5^-\right)\sigma_{-n}\left(z_6^+,z_6^-\right)\right|\mathcal{O}^{\otimes n}\rangle\\ &\simeq\langle\mathcal{O}^{\otimes n}\left|\sigma_n\left(z^+,z^-\right)\sigma_{-n}(1,1)|\mathcal{O}^{\otimes n}\rangle\langle\mathcal{O}^{\otimes n}|\sigma_n\left(z_5^+,z_5^-\right)\sigma_{-n}\left(z_6^+,z_6^-\right)\right|\mathcal{O}^{\otimes n}\rangle,\end{aligned} \tag{A12}$$

in the $\varepsilon\to 0$ limit. By further applying a conformal map

$$\tilde{z}^{\pm}\left(z^{\pm}\right) = \frac{\left(z_1^{\pm}-z^{\pm}\right)z_{64}^{\pm}}{z_{16}^{\pm}\left(z^{\pm}-z_4^{\pm}\right)} \tag{A13}$$

to the second four-point function in Eq. (A12), we get

$$\begin{aligned}\mathrm{tr}\,\rho_{\bar{C}}^n(t) = &\left\{\left(\frac{\beta}{\pi\varepsilon_{\mathrm{UV}}}\right)^4 \sinh\left(\frac{\pi}{\beta}x_{65}^+\right)\sinh\left(\frac{\pi}{\beta}x_{65}^-\right)\sinh\left(\frac{\pi}{\beta}x_{32}^+\right)\sinh\left(\frac{\pi}{\beta}x_{32}^-\right)\right\}^{-2H_n}\\ &\times\left((1-z^+)(1-z^-)\right)^{2H_n}\left\langle\mathcal{O}^{\otimes n}\left|\sigma_n\left(z^+,z^-\right)\sigma_{-n}(1,1)\right|\mathcal{O}^{\otimes n}\right\rangle\\ &\times\left(\left(1-\tilde{z}_5^+\right)\left(1-\tilde{z}_5^-\right)\right)^{2H_n}\left\langle\mathcal{O}^{\otimes n}\left|\sigma_n\left(\tilde{z}_5^+,\tilde{z}_5^-\right)\sigma_{-n}(1,1)\right|\mathcal{O}^{\otimes n}\right\rangle.\end{aligned} \tag{A14}$$

Generally, it is difficult to get a complete analytic expression for the four-point functions since they depend on the details of the dynamics of the theory. However, because we focus on the theory that has a large central charge $c\gg 1$ and a sparse spectrum, the four-point functions can be well approximated by the vacuum Virasoro conformal blocks. Moreover, in evaluating the entanglement entropy by taking the $n\to 1$ limit of the twist operators in the correlator (A14), we only need the heavy–heavy–light–light Virasoro blocks, because the conformal dimension of the twist operators becomes light, $H_n/c\to 0$, $n\to 1$. Upon taking the limit, we keep the conformal dimension $h_{\mathcal{O}}$ of the local operator $\mathcal{O}$, which we assume to be proportional to the central charge $c$, fixed. The dominant contribution of such a four-point function under the limit

is given by [65]

$$\left(\left(1-z^{+}\right)\left(1-z^{-}\right)\right)^{2H_n}\left\langle \mathcal{O}^{\otimes n}\left|\sigma_n\left(z^{+},z^{-}\right)\sigma_{-n}(1,1)\right|\mathcal{O}^{\otimes n}\right\rangle \simeq\left(\frac{\left(z^{+}\right)^{\frac{1-\alpha}{2}}\left(1-\left(z^{+}\right)^{\alpha}\right)\left(z^{-}\right)^{\frac{1-\alpha}{2}}\left(1-\left(z^{-}\right)^{\alpha}\right)}{\alpha^2(1-z^{+})(1-z^{-})}\right)^{-2H_n}, \tag{A15}$$

where $\alpha=\sqrt{1-\frac{24h_{\mathcal{O}}}{c}}=\sqrt{1-\frac{12\Delta}{c}}$. By plugging this result in Eq. (A14) and taking the $n\to 1$ limit, we get the result for the CFT entanglement entropy $S[\bar{C}]=S_\beta[\bar{C}]+\Delta S[\bar{C}]$ with

$$\begin{aligned}
S_\beta[\bar{C}] &= \frac{c}{6}\log\left[\left(\frac{\beta}{\pi\varepsilon_{UV}}\right)^4\sinh\left(\frac{\pi}{\beta}x_{65}^{+}\right)\sinh\left(\frac{\pi}{\beta}x_{65}^{-}\right)\sinh\left(\frac{\pi}{\beta}x_{32}^{+}\right)\sinh\left(\frac{\pi}{\beta}x_{32}^{-}\right)\right]\\
\Delta S[\bar{C}] &= \frac{c}{6}\log\left[\frac{\left(z^{+}\right)^{\frac{1-\alpha}{2}}\left(1-\left(z^{+}\right)^{\alpha}\right)\left(z^{-}\right)^{\frac{1-\alpha}{2}}\left(1-\left(z^{-}\right)^{\alpha}\right)}{\alpha^2\left(1-z^{+}\right)\left(1-z^{-}\right)}\right]\\
&\quad+\frac{c}{6}\log\left[\frac{\left(\tilde{z}_5^{+}\right)^{\frac{1-\alpha}{2}}\left(1-\left(\tilde{z}_5^{+}\right)^{\alpha}\right)\left(\tilde{z}_5^{-}\right)^{\frac{1-\alpha}{2}}\left(1-\left(\tilde{z}_5^{-}\right)^{\alpha}\right)}{\alpha^2\left(1-\tilde{z}_5^{+}\right)\left(1-\tilde{z}_5^{-}\right)}\right].
\end{aligned} \tag{A16}$$

$S_\beta[\bar{C}]$ is the CFT entanglement entropy of the two disjoint intervals at finite temperature $T=1/\beta$ and $\Delta S[\bar{C}]$ is the contribution to the CFT entanglement entropy from the perturbation by the local operator $\mathcal{O}$.[5]

The right-hand side of the above formula (A16) contains branch cuts; therefore, to make it well defined, we need to properly specify the branch. This is achieved by demanding that the resulting entanglement entropy is consistent with causality and positivity of $\Delta S[\bar{C}]$. In imposing these conditions, it is convenient to adopt the quasi-particle picture [47,54,55] for the time evolution of the entanglement entropy in a local quench. It claims the following: By a local quench, a pair of entangled quasi-particles is created, one of which propagates along one spatial direction at the speed of light, the other along the opposite direction.

The change in the CFT entanglement entropy $\Delta S[\bar{C}]$ can be non-zero only when one of such particles is in $\bar{C}$ while the other is not [47–57,63]. This condition constrains possible branches, since vanishing of the entanglement entropy $\Delta S[\bar{C}]=0$ is equivalent to choosing the branch where $(z,z_5)\to 1$ in the $\varepsilon\to 0$ limit. If we have multiple branches satisfying the condition, the intuition coming from the dual holographic setup suggests that we should take the one giving the minimal value of $\Delta S[\bar{C}]$.

In our setup, the causality condition tells us that the CFT entanglement entropy is vanishing in the following three cases: (1) We insert the operator in the domain of dependence of the intervals, i.e., $x_0\in D[\bar{C}_1]$ or $x_0\in D[\bar{C}_2]$. (2) We do not insert the operator in these domains of dependence, but the right-moving particle created by the quench enters $D[\bar{C}_2]$ and the left-mover enters $D[\bar{C}_1]$. (3) We insert the operator in $D[C]$, where $C$ is the complement of $\bar{C}$.

More explicitly, the conditions that the CFT entanglement entropy must vanish in the above regions imply that we should choose the branch $(z^{+},z^{-})\to(1,1)$ and $(\tilde{z}_5^{+},\tilde{z}_5^{-})\to(1,1)$ when the operator $\mathcal{O}$ is inserted at

(I) $D[\bar{C}_1]$: $x_0^{+}<x_3^{+}$, $x_0^{-}<x_3^{-}$,
(II) $D[\bar{C}_2]$: $x_5^{+}<x_0^{+}$, $x_5^{-}<x_0^{-}$,

[5]Note that, if we choose the other channel, then $S_\beta[\bar{C}]$ and $\Delta S[\bar{C}]$ take a different form.

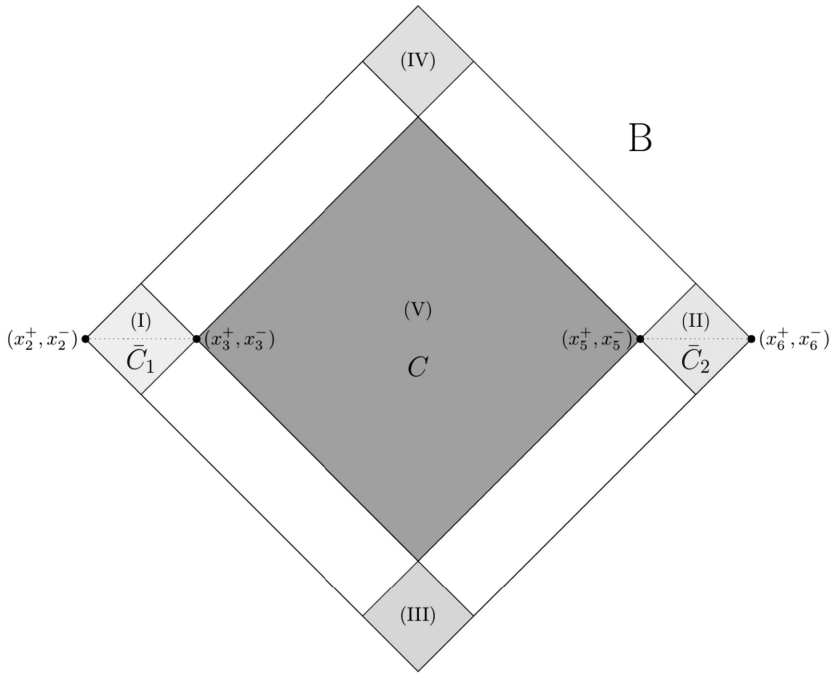


**Fig. A2.** The regions in which $\Delta S[\bar{C}]$ must vanish. The shaded regions correspond to (I)–(V).

(III) Union of the causal pasts of $D[\bar{C}_1]$ and $D[\bar{C}_2]$: $x_0^+ < x_3^+$, $x_5^- < x_0^-$,
(IV) Union of the causal futures of $D[\bar{C}_1]$ and $D[\bar{C}_2]$: $x_5^+ < x_0^+$, $x_0^- < x_3^-$,
(V) $D[C]$: $x_3^+ < x_0^+ < x_5^+$, $x_3^- < x_0^- < x_5^-$.

(See Fig. A2)

The expression of $\Delta S[\bar{C}]$, when the operator is inserted in other regions, is given by suitable analytic continuations of Eq. (A16) in $x_0$ from the above regions (I)–(V). By using the above standard choices, we can determine branch cuts on the other regions from the consistency of the analytic continuation for $x_0^{\pm}$.

We take the region $x_0^+ < x_3^+$ and $x_3^- < x_0^- < x_5$ as an example of such a calculation and determine possible branch choices in the region. Starting from the three regions (I), (III), and (V), which are adjacent to the region $x_0^+ < x_3^+$ and $x_3^- < x_0^- < x_5^-$, we move the operator $\mathcal{O}$ to the region $x_0^+ < x_3^+$ and $x_3^- < x_0^- < x_5^-$. We expand $z^{\pm}$ and $\tilde{z}_5^{\pm}$ to the first order in $\varepsilon$, which is very small compared to $\beta$, and focus on the change of their imaginary parts under the move. For case (I), the imaginary part of $z^-$ changes sign from plus to minus at $x_0^- = x_3^-$, but the others do not. In such a case, we choose the branches as $(z^+, z^-) \to (1, e^{2\pi i})$ and $(\tilde{z}_5^+, \tilde{z}_5^-) \to (1, 1)$. For case (III), the imaginary part of $\tilde{z}_5^-$ changes sign from plus to minus $x_0^- = x_5^-$, but the others do not. Similarly, we choose the branches as $(z^+, z^-) \to (1, 1)$ and $(\tilde{z}_5^+, \tilde{z}_5^-) \to (1, e^{2\pi i})$. For case (V), the imaginary part of $z^+$ changes sign from minus to plus at $x_0^+ = x_3^+$, but the others do not. In this case, we choose the branches as $(z^+, z^-) \to (e^{2\pi i}, 1)$ and $(\tilde{z}_5^+, \tilde{z}_5^-) \to (1, 1)$. By the above calculation, we have finished determining possible branch choices in the region $x_0^+ < x_3^+$ and $x_3^- < x_0^- < x_5^-$.

Having specified the branch cuts in the region, we can calculate the analytic expression for $\Delta S[\bar{C}]$ in the region. Each branch cut gives a different $\Delta S[\bar{C}]$ and, as noted before, we must pick up the dominant contribution corresponding to the minimum $\Delta S[\bar{C}]$ in the region [50]. For example, we focus on the region $x_0^+ < x_3^+$ and $x_3^- < x_0^- < x_5$ and calculate $\Delta S[\bar{C}]$. In this

region, $x_0^+ < x_3^+$ and $x_3^- < x_0^- < x_5^-$, we must compare the above three branch choices obtained from the three regions (I), (III), and (V) and choose the minimum one. This gives

$$\Delta S[\bar{C}] = \frac{c}{6}\log\left[\frac{\beta}{\pi\varepsilon}\frac{\sin\pi\alpha}{\alpha}\frac{\sinh\left(\frac{\pi}{\beta}\left(x_3^+ - x_0^+\right)\right)\sinh\left(\frac{\pi}{\beta}\left(x_0^+ - x_2^+\right)\right)}{\sinh\left(\frac{\pi}{\beta}\left(x_3^+ - x_2^+\right)\right)}\right]$$
$$\text{for the region } x_0^+ < x_3^+ \text{ and } x_3^- < x_0^- < x_5^-. \tag{A17}$$

Similar results hold for the other regions. By combining the above results and $S_\beta[\bar{C}]$, we get the final expression for the entire region in universe $B$.

We have focused on the CFT entanglement entropy of two disjoint intervals. However, we can easily extend the above analysis to the single interval case by removing either region $\bar{C}_1$ or $\bar{C}_2$ and following a similar procedure.

## References


[1] A. Almheiri, R. Mahajan, J. Maldacena, and Y. Zhao, J. High Energy Phys. **2003**, 149 (2020) [arXiv:1908.10996 [hep-th]] [Search inSPIRE].
[2] A. Almheiri, N. Engelhardt, D. Marolf, and H. Maxfield, J. High Energy Phys. **1912**, 063 (2019) [arXiv:1905.08762 [hep-th]] [Search inSPIRE].
[3] G. Penington, J. High Energy Phys. **2009**, 002 (2020) [arXiv:1905.08255 [hep-th]] [Search inSPIRE].
[4] G. Penington, S. H. Shenker, D. Stanford, and Z. Yang; arXiv:1911.11977 [hep-th] [Search inSP IRE].
[5] A. Almheiri, T. Hartman, J. Maldacena, E. Shaghoulian, and A. Tajdini, J. High Energy Phys. **2005**, 013 (2020) [arXiv:1911.12333 [hep-th]] [Search inSPIRE].
[6] S. Ryu and T. Takayanagi, Phys. Rev. Lett. **96**, 181602 (2006) [arXiv:hep-th/0603001 ] [Search inSP IRE].
[7] S. Ryu and T. Takayanagi, J. High Energy Phys. **0608**, 045 (2006) [arXiv:hep-th/0605073 ] [Search inSPIRE].
[8] V. E. Hubeny, M. Rangamani, and T. Takayanagi, J. High Energy Phys. **0707**, 062 (2007) [arXiv:0705.0016 [hep-th]] [Search inSPIRE].
[9] T. Faulkner, A. Lewkowycz, and J. Maldacena, J. High Energy Phys. **1311**, 074 (2013) [arXiv:1307.2892 [hep-th]] [Search inSPIRE].
[10] N. Engelhardt and A. C. Wall, J. High Energy Phys. **1501**, 073 (2015) [arXiv:1408.3203 [hep-th]] [Search inSPIRE].
[11] D. N. Page, Phys. Rev. Lett. **71**, 3743 (1993) [arXiv:hep-th/9306083 ] [Search inSPIRE].
[12] D. N. Page, J. Cosmol. Astropart. Phys. **1309**, 028 (2013) [arXiv:1301.4995 [hep-th]] [Search inSP IRE].
[13] A. Almheiri, T. Hartman, J. Maldacena, E. Shaghoulian, and A. Tajdini, Rev. Mod. Phys. **93**, 035002 (2021) [arXiv:2006.06872 [hep-th]] [Search inSPIRE].
[14] V. Balasubramanian, A. Kar, O. Parrikar, G. Sárosi, and T. Ugajin, J. High Energy Phys. **2101**, 177 (2021) [arXiv:2003.05448 [hep-th]] [Search inSPIRE].
[15] M. Rozali, J. Sully, M. Van Raamsdonk, C. Waddell, and D. Wakeham, J. High Energy Phys. **2005**, 004 (2020) [arXiv:1910.12836 [hep-th]] [Search inSPIRE].
[16] H. Z. Chen, R. C. Myers, D. Neuenfeld, I. A. Reyes, and J. Sandor, J. High Energy Phys. **2010**, 166 (2020) [arXiv:2006.04851 [hep-th]] [Search inSPIRE].
[17] H. Z. Chen, R. C. Myers, D. Neuenfeld, I. A. Reyes, and J. Sandor, J. High Energy Phys. **2012**, 025 (2020) [arXiv:2010.00018 [hep-th]] [Search inSPIRE].
[18] I. Akal, Y. Kusuki, N. Shiba, T. Takayanagi, and Z. Wei, Phys. Rev. Lett. **126**, 061604 (2021) [arXiv:2011.12005 [hep-th]] [Search inSPIRE].
[19] H. Geng, A. Karch, C. Perez-Pardavila, S. Raju, L. Randall, M. Riojas, and S. Shashi, SciPost Phys. **10**, 103 (2021) [arXiv:2012.04671 [hep-th]] [Search inSPIRE].
[20] K. Kawabata, T. Nishioka, Y. Okuyama, and K. Watanabe, J. High Energy Phys. **2105**, 062 (2021) [arXiv:2102.02425 [hep-th]] [Search inSPIRE].

[21] H. Geng, Y. Nomura, and H. Y. Sun, Phys. Rev. D **103**, 126004 (2021) [arXiv:2103.07477 [hep-th]] [Search inSPIRE].
[22] S. Fallows and S. F. Ross, J. High Energy Phys. **2107**, 022 (2021) [arXiv:2103.14364 [hep-th]] [Search inSPIRE].
[23] L. Anderson, O. Parrikar, and R. M. Soni, J. High Energy Phys. **2021**, 226 (2020) [arXiv:2103.14746 [hep-th]] [Search inSPIRE].
[24] T. Li, J. Chu, and Y. Zhou, J. High Energy Phys. **2011**, 155 (2020) [arXiv:2006.10846 [hep-th]] [Search inSPIRE].
[25] I. Akal; arXiv:2010.12565 [hep-th] [Search inSPIRE].
[26] F. Deng, J. Chu, and Y. Zhou, J. High Energy Phys. **2103**, 008 (2021) [arXiv:2012.07612 [hep-th]] [Search inSPIRE].
[27] A. Bhattacharya, A. Bhattacharyya, P. Nandy, and A. K. Patra, J. High Energy Phys. **2105**, 135 (2021) [arXiv:2103.15852 [hep-th]] [Search inSPIRE].
[28] V. Balasubramanian, A. Kar, and T. Ugajin, J. High Energy Phys. **2102**, 136 (2021) [arXiv:2008.05274 [hep-th]] [Search inSPIRE].
[29] V. Balasubramanian, A. Kar, and T. Ugajin, J. High Energy Phys. **2102**, 072 (2021) [arXiv:2008.05275 [hep-th]] [Search inSPIRE].
[30] T. Hartman, Y. Jiang, and E. Shaghoulian, J. High Energy Phys. **2011**, 111 (2020) [arXiv:2008.01022 [hep-th]] [Search inSPIRE].
[31] Y. Chen, V. Gorbenko, and J. Maldacena, J. High Energy Phys. **2102**, 009 (2021) [arXiv:2007.16091 [hep-th]] [Search inSPIRE].
[32] W. Sybesma, Classical Quantum Gravity **38**, 145012 (2021) [arXiv:2008.07994 [hep-th]] [Search in SPIRE].
[33] C. G. Callan, Jr, S. B. Giddings, J. A. Harvey, and A. Strominger, Phys. Rev. D **45**, R1005 (1992) [arXiv:hep-th/9111056 ] [Search inSPIRE].
[34] T. M. Fiola, J. Preskill, A. Strominger, and S. P. Trivedi, Phys. Rev. D **50**, 3987 (1994) [arXiv:hep-th/9403137 ] [Search inSPIRE].
[35] J. G. Russo, L. Susskind, and L. Thorlacius, Phys. Lett. B **292**, 13 (1992) [arXiv:hep-th/9201074 ] [Search inSPIRE].
[36] K. Hashimoto, N. Iizuka, and Y. Matsuo, J. High Energy Phys. **2006**, 085 (2020) [arXiv:2004.05863 [hep-th]] [Search inSPIRE].
[37] T. Hartman, E. Shaghoulian, and A. Strominger, J. High Energy Phys. **2007**, 022 (2020) [arXiv:2004.13857 [hep-th]] [Search inSPIRE].
[38] T. Anegawa and N. Iizuka, J. High Energy Phys. **2007**, 036 (2020) [arXiv:2004.01601 [hep-th]] [Search inSPIRE].
[39] C. Krishnan, V. Patil, and J. Pereira; arXiv:2005.02993 [hep-th] [Search inSPIRE].
[40] F. F. Gautason, L. Schneiderbauer, W. Sybesma, and L. Thorlacius, J. High Energy Phys. **2005**, 091 (2020) [arXiv:2004.00598 [hep-th]] [Search inSPIRE].
[41] Y. Matsuo, J. High Energy Phys. **2107**, 051 (2021) [arXiv:2011.08814 [hep-th]] [Search inSPIRE].
[42] X. Wang, R. Li, and J. Wang, J. High Energy Phys. **2104**, 103 (2021) [arXiv:2101.06867 [hep-th]] [Search inSPIRE].
[43] X. Wang, R. Li, and J. Wang, Phys. Rev. D **103**, 126026 (2021) [arXiv:2104.00224 [hep-th]] [Search inSPIRE].
[44] H. Geng, S. Lüst, R. K. Mishra, and D. Wakeham, J. High Energy Phys. **2108**, 003 (2021) [arXiv:2104.07039 [hep-th]] [Search inSPIRE].
[45] V. Balasubramanian, A. Kar, and T. Ugajin; arXiv:2104.13383 [hep-th] [Search inSPIRE].
[46] J. Maldacena and L. Susskind, Fortschr. Phys. **61**, 781 (2013) [arXiv:1306.0533 [hep-th]] [Search in SPIRE].
[47] P. Calabrese and J. Cardy, J. Stat. Mech. **0710**, P10004 (2007) [arXiv:0708.3750[cond-mat.stat-mech]] [Search inSPIRE].
[48] P. Caputa, M. Nozaki, and T. Takayanagi, Prog. Theor. Exp. Phys. **2014**, 093B06 (2014) [arXiv:1405.5946 [hep-th]] [Search inSPIRE].
[49] M. Nozaki, T. Numasawa, and T. Takayanagi, J. High Energy Phys. **1305**, 080 (2013) [arXiv:1302.5703 [hep-th]] [Search inSPIRE].
[50] C. T. Asplund, A. Bernamonti, F. Galli, and T. Hartman, J. High Energy Phys. **1502**, 171 (2015) [arXiv:1410.1392 [hep-th]] [Search inSPIRE].

[51] P. Caputa, J. Simón, A. Štikonas, T. Takayanagi, and K. Watanabe, J. High Energy Phys. **1508**, 011 (2015) [arXiv:1503.08161 [hep-th]] [Search inSPIRE].
[52] T. Ugajin; arXiv:1311.2562 [hep-th] [Search inSPIRE].
[53] C. T. Asplund and A. Bernamonti, Phys. Rev. D **89**, 066015 (2014) [arXiv:1311.4173 [hep-th]] [Se arch inSPIRE].
[54] M. Nozaki, T. Numasawa, and T. Takayanagi, Phys. Rev. Lett. **112**, 111602 (2014) [arXiv:1401.0539 [hep-th]] [Search inSPIRE].
[55] M. Nozaki, J. High Energy Phys. **1410**, 147 (2014) [arXiv:1405.5875 [hep-th]] [Search inSPIRE].
[56] P. Caputa, J. Simón, A. Štikonas, and T. Takayanagi, J. High Energy Phys. **1501**, 102 (2015) [arXiv:1410.2287 [hep-th]] [Search inSPIRE].
[57] J. R. David, S. Khetrapal, and S. P. Kumar, J. High Energy Phys. **1608**, 127 (2016) [arXiv:1605.05987 [hep-th]] [Search inSPIRE].
[58] T. J. Hollowood and S. P. Kumar, J. High Energy Phys. **2008**, 094 (2020) [arXiv:2004.14944 [hep-th]] [Search inSPIRE].
[59] K. Goto, T. Hartman, and A. Tajdini, J. High Energy Phys. **2104**, 289 (2021) [arXiv:2011.09043 [hep-th]] [Search inSPIRE].
[60] H. Z. Chen, Z. Fisher, J. Hernandez, R. C. Myers, and S. M. Ruan, J. High Energy Phys. **2003**, 152 (2020) [arXiv:1911.03402 [hep-th]] [Search inSPIRE].
[61] H. Z. Chen, Z. Fisher, J. Hernandez, R. C. Myers, and S. M. Ruan, J. High Energy Phys. **2101**, 065 (2021) [arXiv:2007.11658 [hep-th]] [Search inSPIRE].
[62] T. J. Hollowood, S. Prem Kumar, and A. Legramandi, J. Phys. A **53**, 475401 (2020) [arXiv:2007.04877 [hep-th]] [Search inSPIRE].
[63] T. Hartman, S. Jain, and S. Kundu, J. High Energy Phys. **1605**, 099 (2016) [arXiv:1509.00014 [hep-th]] [Search inSPIRE].
[64] Y. Chen, J. High Energy Phys. **2003**, 033 (2020) [arXiv:1912.02210 [hep-th]] [Search inSPIRE].
[65] A. L. Fitzpatrick, J. Kaplan, and M. T. Walters, J. High Energy Phys. **1408**, 145 (2014) [arXiv:1403.6829 [hep-th]] [Search inSPIRE].